Investigating the effects of different natural molecules on the structure and oligomerization propensity of hen egg-white lysozyme

Ali Chaari, Christine Fahy, Alexandre Chevillot-Biraud, Mohamed Rholam

Investigating the effects of different natural molecules on the structure and oligomerization propensity of hen egg-white lysozyme

Ali Chaari[1,2,*#], Christine Fahy[1], Alexandre Chevillot-Biraud[1] and Mohamed Rholam[1,]

[1] ITODYS, UMR CNRS 7086, Univ. Paris Diderot, Sorbonne Paris Cité, 75205 Paris, France.

[2] Laboratoire de Génétique et Biologie Cellulaire, Université de Versailles Saint-Quentin-en-Yvelines, 78035 Versailles, France.

[#] **Corresponding author.** Ali Chaari

Premedical department_Weill Cornell Medicine in Qatar

Qatar Foundation-Education City, P.O.Box 24144, Doha, Qatar

Phone: +974-4492-8431

E-mail address: alc2033@qatar-med.cornell.edu.

[*] **Present address.** Ali Chaari

Premedical department_Weill Cornell Medicine in Qatar

Qatar Foundation-Education City, P.O.Box 24144, Doha, Qatar

Phone: +974-4492-8431

E-mail address: alc2033@qatar-med.cornell.edu.

Abbreviations:

HEWL: Hen Egg White Lysozyme

ThT: Thioflavin T

Trp: Tryptophan

AFM: Atomic Force Microscopy

DLS: Dynamic Light Scattering

ATR-FTIR: Attenuated Total Reflectance-Fourier Transform Infrared

Keywords: Aggregation kinetics; Amyloidosis; Aggregation inhibitors; Anti-amyloidogenic; Hen-egg-white lysozyme; Natural compounds.

Abstract

The formation of amyloid aggregates is the hallmark of systemic and neurodegenerative diseases, also known as amyloidosis. Many proteins have been found to aggregate into amyloid-like fibrils and thus process is recognized as general tendency of polypeptides. Inhibition of protein aggregation and fibril formation is thus one of the important strategies in the prevention and treatment of such disease. There is a growing interest of identification of small molecules mainly natural compounds that can prevent or delay amyloid fibril formation. In this work, we report the effect of various compounds from different groups on the amyloid fibrillation of hen egg white lysozyme, a model protein for amyloid formation. Herein, a range of biophysical techniques have been employed in order to establish a systematic approach to study the effect of candidate inhibitors on amyloid aggregation.

Results demonstrated that the strategy used show that the different techniques are complimentary in order to elucidate a complete in vitro picture of the effect of the used compounds on HEWL aggregation. Moreover, compared to the data obtained by other groups for the inhibition of lysozyme fibril formation, this work provides new insights into the structural changes (local, secondary, oligomeric, fibrillar structures) undergone by HEWL during aggregation in the presence and absence of inhibitors.

Introduction

Protein misfolding and amyloid formation are an underlying pathological hallmark in a number of relevant diseases ranging from neurological disorders (i.e. Alzheimer's and Parkinson's diseases) to various systematic amyloidosis (Hutt, Powers, and Balch 2009; Hartl 2017; Lindner and Demarez 2009; Chiti and Dobson 2006; Selkoe 2004). Irrespective of their sequence or tertiary structure, the proteins, involved in these diseases, generate fibrillar aggregates exhibiting common morphological features (Alam et al. 2017; Jiménez et al. 2001; Chamberlain et al. 2000). Moreover, these characteristics were also observed for the fibril-like aggregates obtained under appropriate conditions (i.e. extreme pH, heating and the presence of cosolvent etc...) for non-disease-related proteins (M. V. Khan et al. 2015; Lomakin et al. 1996; Ruzafa et al. 2012; Jayaraman et al. 2012; Swaminathan et al. 2011; Jean et al. 2008; Grudzielanek et al. 2007; Grondelle et al. 2007). Together, these observations have led to the conclusion that the ability to form amyloid aggregates is an intrinsic property of the polypeptide chains of proteins (Uversky and Fink 2004), and that all amyloid proteins may exhibit similar structure-specific cytotoxic effects through common mechanisms (Kayed et al. 2003; Bucciantini et al. 2002). Hence, regardless of the mode of pathogenesis of these amyloid proteins, inhibition and/or reversion of the aggregation and amyloid fibril formation of these proteins has emerged as a possible therapeutic strategy for the prevention and treatment of amyloid diseases (R. Liu et al. 2012; DaSilva, Shaw, and McLaurin 2010; Florent-Béchard et al. 2009; Cavalli et al. 2008).

A large number of diverse compounds have been found to inhibit or reduce the aggregation/fibrillogenesis of the amyloid-forming proteins and/or the cytotoxicity triggered by these amyloid proteins (Scarpini, Galimberti, and Ghezzi 2013; Amijee et al. 2009). These compounds or molecules include antibodies (Legleiter et al. 2004), chaperone proteins (Lee et al.

2005; Santhoshkumar and Sharma 2004), synthetic peptides (Kumar, Namsechi, and Sim 2015; Dolphin et al. 2007), nanoparticles (Ishtikhar et al. 2015; Cabaleiro-Lago, Szczepankiewicz, and Linse 2012) and small organic substances (Di Giovanni et al. 2010; Gazova et al. 2013; Stefani and Rigacci 2013; Alam et al. 2016; Leong et al. 2009; Siddiqi et al. 2017; Porat, Abramowitz, and Gazit 2006; Masuda et al. 2006). Among these latter compounds, the natural molecules from various sources have received a great interest as alternative candidates for the development of amyloid aggregation inhibitors against the human diseases (Galleano et al. 2010; Q. Liu et al. 2007; Ono et al. 2006; Moran 2013; Baur and Sinclair 2006). For examples, curcumin and resveratrol are typical examples of the natural molecules that have been reported to exert an inhibitory effect on the aggregation of diverse amyloid proteins such as amyloid β-peptide, α-synuclein, transthyretin, islet amyloid polypeptide or lysozyme (Stefani and Rigacci 2013; Alam et al. 2016; Leong et al. 2009; Siddiqi et al. 2017; Porat, Abramowitz, and Gazit 2006; Masuda et al. 2006). Besides their anti-amyloidogenic activity, these molecules exhibit anti-oxidative and anti-inflammatory properties (Ono et al. 2006; Moran 2013; Baur and Sinclair 2006). Although several small molecule inhibitors of protein self-assembly have been identified, their mechanisms of action are often still unclear, and their effects can vary depending on the conditions in which they are assessed such as the point at which these inhibitors intercede within the assembly process of proteins, the protein/inhibitor molar ratio, the pH or the temperature.

In our previous study ,we have analyzed the self-assembly of hen egg-white lysozyme, a well-known model protein commonly utilized for the study of protein aggregation (Chaari et al. 2015; J. M. Khan et al. 2014; Raccosta, Martorana, and Manno 2012; Gharibyan et al. 2007; Dumoulin, Kumita, and Dobson 2006), by using complementary methods which provided new insights into the structural changes (local, secondary, oligomeric/fibrillar structures) undergone by the lysozyme under agitation during a prolonged heating in acidic pH. In view of the above

observations, we have used the same aggregation conditions and adopted the same experimental approach to investigate the influence of different natural compounds on the fibril formation of HEWL with the aim to characterize their effects on the kinetics of aggregation and to evaluate their anti-aggregating and anti-amyloidogenic activities against the formation of oligomeric/fibrillar species.

Materials and Methods

Materials

Hen egg-white lysosyme (EC 3.2.1.17) and thioflavin T were purchased from Sigma-Aldrich (St. Louis, MO). The natural molecules (resveratrol, tyrosol, rutin, nicotine and dopamine) were purchased from sigma All other reagents and buffer components were of analytical grade.

Lysozyme aggregation

The sample solutions of hen egg white lysozyme (HEWL), without further purification, were prepared in 10 mM glycine buffer (pH 2.0) containing 0.2% (w/v) sodium azide. To produce the amyloid structures, HEWL solutions (20 mg/ml) were incubated for different days at 55°C in a thermomixer with an agitation of 700 rpm. At regular time intervals, samples for analysis were taken and stored at 4°C. HEWL concentrations were determined from UV absorption measured at λ =280 nm (ε_{280} = 2.64 ml.mg^{-1}.cm^{-1}).

Compound testing

All Compounds were dissolved in dimethylsulfoxide (DMSO) and kept as stock solutions at -20°C in order to maintain their maximal stability. During the experiments, they were used immediately after unfreezing and kept away from light. To assay for inhibitory activity, each compound was added to the monomeric HEWL solution (20 mg/ml) in 10 mM glycine buffer (pH 2.0) containing 0.2% (w/v) sodium azide at the start of HEWL aggregation with an agitation of 700 rpm at 55°C.

Thioflavin T (ThT) fluorescence assay

To monitor the aggregation of lysozyme, in the absence or the presence of each compound, the fluorescent ThT dye was added to the protein samples (10 µM) to a final concentration of 20 µM. The fluorescence emission spectra of ThT were collected from 450 nm to 550 nm on a

Bowman fluorescence spectrophotometer using an excitation wavelength of 440 nm. Fluorescence measurements were performed at 25°C in 1 cm quartz cell with both excitation and emission bandwidths of 5 nm. The fluorescence spectra of ThT blanks, in the absence or presence of each ligand, were independently measured and subtracted from the corresponding fluorescence spectra of HEWL samples. The values of the quantum yield of ThT fluorescence, determined by integrating the emission spectra from 450 nm to 500 nm, are the mean of three measurements, each performed in quadruplicate.

Atomic Force Microscopy (AFM) measurements

AFM images were acquired in non-contact mode in a vibration-insulated environment using a PicoPlus microscope (Molecular Imaging) equipped with a NanoScan-3000 controller. For imaging, we used single beam aluminium-coated cantilevers (type NSC36/ALBS, μmasch) with Rc<10 nm, 110-130 μm lengths and nominal spring constant (0.6 N/m). The drive frequency was between 200 and 400 kHz. The solutions of HEWL, alone or in the presence of ligands, were diluted 400 times and a small aliquot (20 μl) was deposited on freshly cleaved mica. The samples were incubated on mica for 10 min followed by three washes with 50 μl water to gently remove the material not adsorbed to the substrate. Each sample was dried under mild vacuum and imaged in air. Each experiment was performed in quadruplicate at 25°C. The acquisition and the analysis of AFM pictures were performed by using the softwares “Nanoscope 5.30r3sr3” and “WSxM 5.0 Develop 3.1”, respectively.

Dynamic Light Scattering (DLS) measurements

DLS measurements were carried out using a DynaPro MS800 instrument (Wyatt Technologies Corp.) equipped with a gallium aluminium arsenide 825 nm laser. The total light scattering intensity of HEWL solutions (1 mg/ml), alone or in the presence of ligands, was collected at a 90° angle. All measurements were made in 3 mm quartz cell at 25°C. The

acquisition of data (usually 30–40 points) was made with an acquisition time of 30 s and the obtained data were averaged. The autocorrelation curves were deconvoluted using Dynamics V6 software to obtain the size distribution and the hydrodynamic radii (<R_h>). Each experiment was repeated three times to ensure reproducibility.

Fourier Transform Infra Red spectroscopy (FTIR) analysis

Attenuated total reflectance Fourier transform infrared (ATR-FTIR) spectra of HEWL samples, in the absence or the presence of each compound, were recorded on a FTIR spectrometer (model IFS-66v; Nicolett) equipped with a horizontal ZnS ATR accessory. 50 µl of samples (1 mg/ml) were placed directly in the ZnS ATR accessory and the spectra were recorded at 25°C. 200 scans were performed for each spectrum at 2 cm^{-1} resolution. The spectrum of buffer background, containing each ligand alone, was independently measured and subtracted from the corresponding protein spectrum before curve fitting of the amide I region. Each experiment was repeated three times to ensure reproducibility. To identify the different spectral components of HEWL species and to determine their respective content, the spectra were analyzed by using the Grams 31 program version 4.14 (Galactic Industries Corporation, Salem, NH).

Intrinsic fluorescence assay

The fluorescence emission spectra (collected from 300 nm to 500 nm) of 20-fold diluted lysozyme samples, in the absence or the presence of compounds, were acquired with a Bowman fluorescence spectrophotometer. The excitation wavelength was set at 295 nm in order to observe exclusively the fluorescence of Trp residues. Fluorescence measurements were performed at 25°C in 1 cm quartz cell with both excitation and emission bandwidths of 2 nm. The fluorescence spectra of protein samples were determined by subtracting the fluorescence of buffer, in the absence or presence of each ligand, and corrected for scattering effect (Eftink

1991). Each experiment was performed in quadruplicate. The values of the quantum yield of Trp fluorescence were determined by integrating the fluorescence emission spectra from 310 nm to 450 nm.

Analysis of fibril formation kinetics

All aggregation curves were fitted to a sigmoidal function (Morris, Watzky, and Finke 2009), implemented within the Origin 8.0 software package (Microcal, Southampton, MA), to extract the relevant aggregation parameters (see Equation 1).

$$S = S_i + [S_f - S_i] / [1 + \exp^{(t - t1/2)/\tau}] \qquad (1)$$

where S is the signal observed at the time t, S_i and S_f are the initial and final values of the signal, respectively. The values of the parameters of the sigmoidal curve $t_{1/2}$ (half-time: time required to reach the half of the maximum of the signal S_f) and τ (magnitude of the signal change) were determined by fitting the experimental data by non-linear least-square method.

Analysis of fibril formation inhibition

Concentration-effect data from the ThT fluorescence assays were fitted to a sigmoidal function [**53]**, implemented within the Origin 8.0 software package (Microcal, Southampton, MA), to extract the relevant inhibition parameters (see Equation (2)).

$$F = F_{min} + [F_{max} - F_{min}] / [1 + 10^{(\log IC50 - \log x)/n}] \qquad (2)$$

where F is the fluorescence quantum yield of ThT in the presence of inhibitor at concentration x, F_{max} and F_{min} represent the maximum and minimum of the fluorescence quantum yield of ThT in the absence and presence of inhibitors, respectively. The values of the parameters n (Hill coefficient) and IC_{50} (the concentration of inhibitor that results in 50% of maximal inhibition) were determined by fitting the experimental data by non-linear least-square method.

Results and Discussion

Because diverse small organic molecules have been found to reduce the formation of amyloidogenic forms of proteins (oligomers and protofibrils) and/or to disperse the preformed fibrils (Q. Liu et al. 2007; Ono et al. 2006; Moran 2013; Baur and Sinclair 2006; Chaari et al. 2015; J. M. Khan et al. 2014; Raccosta, Martorana, and Manno 2012; Gharibyan et al. 2007; Dumoulin, Kumita, and Dobson 2006), we have evaluated here the inhibiting potential of five structurally different natural compounds (Fig 1) against the formation of oligomeric/fibrillar species of HEWL under our aggregation conditions (see material and methods). To this end, we have used different methods including various spectroscopic techniques (e.g. thioflavin T (ThT) fluorescence spectroscopy, attenuated total reflectance (ATR)-Fourier transform infrared (FTIR) spectroscopy, dynamic light scattering (DLS) and tryptophan (Trp) fluorescence spectroscopy) and atomic force microscopy (AFM).

I. Inhibition of the formation of lysozyme amyloid aggregates by natural compounds.

To confirm the ability of resveratrol and tyrosol (polyphenols), rutin (flavonol), nicotine (alkaloid) and dopamine (catecholamine) to inhibit the formation of HEWL fibrils, we have investigated the structural features of HEWL species generated at the end point of the equilibrium phase by each ligand for the drug-to-protein molar ratio of 1:1.

I.1. Morphological characterization of ligand-generated species of HEWL

Firstly, the generated HEWL species were morphologically probed by the atomic force microscopy (AFM) which is a method generally used to characterize the size and shape of aggregates for many proteins (Jiménez et al. 2001; Chamberlain et al. 2000).

Fig 2 exhibits the AFM images obtained for the products of the 264 hrs incubation of HEWL with and without the ligands at low pH (~2.0) and high temperature (55°C) under agitated condition (~700 rpm). As shown in the Fig 2A, the incubation of HEWL sample alone leads predominantly to the formation of fibrillar aggregates exhibiting different lengths (>100 nm) in agreement with our previous reports (Dumoulin, Kumita, and Dobson 2006). On the contrary, such fibrillar structures were not observed in the AFM images of HEWL samples containing the resveratrol (Fig 2B), the tyrosol (Fig 2C), the rutin (Fig 2D), the nicotine (Fig 2E) or the dopamine (Fig 2F), indicating that the tested compounds are able to prevent the formation of HEWL fibrillar aggregates. Moreover, these generated HEWL species present differences at the level of their morphologies compared to the freshly prepared lysozyme sample devoid of aggregated/fibrillar species (Gharibyan et al. 2007). Indeed, the end-products of the aggregation reaction exhibit essentially round spherical structures.

The table 1 summarizes the size and distribution of these oligomeric products deduced from the analysis of AFM images by softwares (see material and methods). The analysis of these data allows us to deduce the following observations on the effects of these compounds. Firstly, the majority of the oligomers produced by all the ligands (>80%) were shorter than 30 nm in length with a higher percentage for the HEWL species generated by the nicotine (~100%). Secondly, the nicotine generates HEWL aggregates essentially shorter than 15 nm in length (~89%) whereas those produced by the dopamine, rutin and resveratrol compounds have predominantly lengths situated between 15 and 30 nm (>60%). Thirdly, the tyrosol-generated aggregates exhibit a polydisperse size distribution despite the amount of the aggregate species having a length shorter than 15 nm (~47%) is somewhat higher than the percentage of those having a length shorter than 30 nm (~34%). Finally, the rutin and dopamine, compounds, which belong to two different chemical classes, exhibit the same size distribution whereas the resveratrol and the

tyrosol, belonging to the same chemical class, display a different and opposite size distribution. Overall, these AFM results demonstrate that all the compounds have distinctive inhibitory effects on the formation of HEWL fibrils by generating small oligomeric species which exhibit differences at level of their size distribution**.**

I.2. Structural features of ligand-generated species of HEWL

Given that the fibrillar aggregates of many proteins were shown to harbour high β-sheet contents (Alam et al. 2017; Jiménez et al. 2001), the secondary structures of the generated HEWL species were examined by the attenuated total reflectance Fourier-transform infrared (ATR-FTIR) spectroscopy, which is a method particularly suitable to the study of protein aggregates (Krimm and Bandekar 1986).

Fig 3 exhibits the ATR-FTIR spectra of the end-products of the 264 hrs incubation of HEWL with each ligand at low pH (~2.0) and high temperature (55°C) under agitated condition (~700 rpm). As shown, the HEWL samples, treated with an equimolar concentration of the nicotine (Fig 3A), tyrosol (Fig 3B), rutin (Fig 3C), dopamine (Fig 3D) and resveratrol (Fig 3E) molecules, exhibit significant differences at level of the shape of their ATR-FTIR spectra. Firstly, while the amide II region of all spectra exhibits a single maximum intensity (AII_1), the amide I region of spectra (located between 1600-1700 cm^{-1}) displays a single maximum intensity (AI_1) for the nicotine and two maximum intensities (AI_1 and AI_2) for the other compounds. Secondly, the value of the ratio [AI_1/AII_1] is slightly inferior to 1 for the tyrosol- and nicotine-generated species of HEWL whereas it is superior to 1 for the HEWL species generated by the rutin, resveratrol and dopamine compounds. Thirdly, the value of the ratio [AI_1/AI_2] is somewhat superior to 1 for the resveratrol-containing HEWL sample whereas it was found to be ~1.4, ~1.6 and ~1.9 for the HEWL samples containing the dopamine, the rutin and the tyrosol, respectively. This qualitative analysis of infrared spectra reveals substantial

differences between the conformations of generated HEWL species resulting from the distinctive inhibitory effects of these compounds on the assembly of HEWL monomers.

Since the amide I region of the infrared spectra of proteins is very sensitive to changes in their secondary structures (Surewicz and Mantsch 1988; Byler and Susi 1986), the deconvolution and curve-fitting of this spectral region for the HEWL spectra (Fig 3) were used to evaluate the percentage of content in each secondary structure type, as listed in Table 2. Compared to the compositions of β-sheet and α-helix observed for the monomers and fibrils of HEWL alone (Dumoulin, Kumita, and Dobson 2006), these data indicate that the secondary structure contents of the resulting species of the protein are mostly changed by the tested compounds**.** Indeed, the HEWL species generated by all the compounds exhibit a lower amount of β-sheet conformations and a higher percentage of α-helix structures than that of the fibrillar HEWL species (70% and 20%, respectively). In contrast, they display a lower or similar percentage of α-helix and a higher amount of β-sheet conformations than that of the monomeric forms of HEWL (~50% and ~30%, respectively). Moreover, the values of the ratio [α-helix(%)/β-sheet(%)] of the HEWL species generated by all the compounds are situated between those obtained for the monomers (~2.4) and fibrils (~0.3) of the protein alone. Indeed, the ratio [α-helix(%)/β-sheet(%)] is inferior to 1 for the dopamine- and rutin-generated species of HEWL (~0.8) whereas it is superior to 1 for the HEWL samples containing the resveratrol, nicotine and tyrosol compounds (~1.20, ~1.35 and ~1.40, respectively). Although the secondary structures of the generated HEWL species are efficiently modified, this spectroscopic analysis demonstrates that the presence of these compounds clearly prevented the structural transition from the native α-helix rich HEWL conformer to amyloidogenic β-sheet rich species (Morris, Watzky, and Finke 2009).

II. Inhibition effects on the kinetics of HEWL fibril formation.

After shown that the resveratrol, tyrosol, rutin, nicotine and dopamine compounds are able to inhibit the HEWL fibrillar structures formed at the end point of the assembly process (Fig 2,3), their inhibitory potentials were investigated in more details by analysing their effects on the kinetics of the HEWL aggregation/fibrillization at the drug-to-protein molar ratio of 1:1.

II.1. ThT fluorescence analysis

To investigate the effects of each compound on the lysozyme aggregation kinetics, we have analyzed firstly the time dependency of the extent of HEWL aggregation by the ThT fluorescence that is commonly used as a principal index for monitoring the kinetics of protein fibrillogenesis (Levine 2008).

Fig 4 displays the kinetic traces of HEWL aggregation in the absence and presence of resveratrol, tyrosol, rutin, nicotine and dopamine at a concentration equimolar to HEWL monomer (1.4 mM). As evidenced by our results, the ThT fluorescence quantum yield of ligand-containing HEWL samples (as given by the area under the spectra) decreases significantly during the studied time interval of the aggregation of HEWL sample without inhibitor. Moreover, we observed that the presence of DMSO (2.5%), used to facilitate solubilization of these compounds, had a negligible effect on HEWL aggregation (data not shown) and the samples of each ligand alone (at the concentrations used in this study) did not quench the ThT fluorescence (data not shown). Together, these ThT fluorescence data indicate that these compounds exert an attenuating effect on the kinetics of aggregation/fibrillization of HEWL. To better characterize the inhibitory mechanism(s) of these compounds, we have analyzed in details their effects on the kinetic parameters of HEWL aggregation.

Generally, the decrease in the amplitude of the aggregation reactions (steady-state value), the reduction in the rate constant of fibril growth k ($k=1/\tau$) and the extension of the lag time t_{lag} ($t_{lag}=t_{1/2}-2\tau$) have been generally used as positive measures of inhibition of protein aggregation. As shown in the Fig 4, the steady-state value of ThT fluorescence (amplitude) is markedly reduced for all the ligand-containing HEWL samples, indicating a high inhibiting potential of the tested compounds. For example, the calculated percentage of the reduction in the fluorescence quantum yield of ThT (% = 100 × [1 − [ThT fluorescence quantum yield of ligand-containing HEWL sample]/[maximal ThT fluorescence quantum yield of aggregate HEWL]) was found to vary from **~88% in the resveratrol-containing HEWL sample to ~94% in the tyrosol- and dopamine-containing HEWL samples after an incubation of 264 hrs.** Besides affecting the amplitude of the aggregation kinetics, we find that these compounds also affect the rate constant of fibril growth (k) and the lag time (t_{lag}) whose the mean values were extracted from the ThT fluorescence kinetics data (Fig 4) by a nonlinear least square curve-fitting to a sigmoidal function (Morris, Watzky, and Finke 2009). From the analysis of the mean k and t_{lag} values, summarized in the table 3, it can be deduced the following observations. Firstly, the time constant of growth phase of the fibrillation of HEWL alone (τ=~37 hrs) is somewhat reduced by the presence of nicotine, rutin or tyrosol whereas it exhibits a substantial increase for the HEWL solutions containing the resveratrol and dopamine. Interestingly, the higher effects on τ were produced by the dopamine (~51% increase) and tyrosol (~11% decrease). Secondly, the duration of the lag phase of the aggregation of HEWL control sample (t_{lag}=~66 hrs) was reduced by the nicotine and dopamine compounds whereas it was extended by the tyrosol, resveratrol and rutin molecules. It is noteworthy that the higher effects on the length of t_{lag} were produced by the rutin (~48% augmentation) and dopamine (~46% reduction). Thirdly, the effects of nicotine or resveratrol (group I) on the both kinetics parameters are qualitatively similar whereas those of

tyrosol, rutin or dopamine (group II) are opposite. Furthermore, the compounds of each group exhibit between them distinctive effects. For the group I, the mean values of τ and t_{lag} are together augmented by the resveratrol whereas they are reduced by the nicotine. In the case of the group II, the dopamine lessens the growth rate (increase of τ) and shortens the lag time while the resveratrol and rutin enhances the growth rate (decrease of τ) and lengthens the lag time. Our ThT fluorescence analysis demonstrates that all the tested molecules modulate strongly and differently the HEWL fibrillation and oligomerization kinetics and exerts their inhibitory potential by affecting substantially either the length of the nucleation phase (t_{lag}) or the growth rate of the elongation phase (k), or the both kinetics parameters of the HEWL aggregation.

II.2. HEWL fibrillogenesis inhibition as revealed by DLS.

To further investigate the effects of these compounds on the aggregative behaviour of HEWL, the characteristic dimensions of ligand-generated species of HEWL were evaluated via DLS, which is a powerful technique used to monitor the growth of oligomeric particles upon aggregation as well as to determine the size distribution of protein assemblies (Takeuchi et al. 2014).

For illustration, we give the DLS graphs obtained for the products generated at the 264 hrs incubation of HEWL alone (Fig 5A) and with an equimolar concentration of dopamine (Fig 5B), nicotine (Fig 5C), resveratrol (Fig 5D), rutin (Fig 5E) and tyrosol (Fig 5F) and their corresponding hydrodynamic radii that are listed in the table 4. As evidenced by these DLS graphs, the size distribution by mass of HEWL samples displays two peaks corresponding to two types of HEWL species generated by each compound. The smaller of these represents the major population (**~85-90%)** and has a hydrodynamic radius ($<R_h>_M$) which is mainly higher than that obtained for the samples containing unheated lysozyme in the presence of each ligand

(<R_h>=~1.4 nm). Indeed, the <R_h>$_M$ value varies from ~17 nm in the presence of dopamine to ~37 nm in the presence of tyrosol (Table 4). The second type of generated species, corresponding to the larger-particles of ligand-containing HEWL samples, represents the minor population (~**10-15%)** and exhibits elevated hydrodynamic radii (<R_h>$_m$) as the heated lysozyme alone (Table 4). However, the <R_h>$_m$ value of HEWL samples containing the rutin, nicotine or tyrosol molecules is elevated compared to that found for the aggregated lysozyme (<R_h>=~145 nm) whereas that of HEWL samples containing the dopamine or resveratrol compounds is lower (Table 4). These DLS data reveal that these small organic compounds prevent the formation of HEWL fibrils by generating two types of species at the end of the self-assembly pathway of HEWL.

As previously observed for the size distribution plots of the resulting species of the 264 hrs incubation of HEWL with each compound (Fig 5B-F), we find that those of HEWL products, generated at each time point of the course of HEWL aggregation, also displays two peaks (data not shown). For example, the table 5 summarizes the hydrodynamic radius and amount values of the two types of HEWL species detected at certain time points along the self-assembly pathway of HEWL. Interestingly, we observe that while the hydrodynamic radius of both HEWL species increased with the incubation time their amounts are variable during the aggregation process. By taking into account of these mentioned observations, we have used the temporal evolution of the hydrodynamic radius (<R_h>$_M$) of the smallest-particle population of ligand-containing HEWL samples (Fig 6) to draw some general conclusions about the effects of these compounds on the kinetics of HEWL aggregation**.** As shown, the initial <R_h>$_M$ of ligand-containing HEWL samples (~1.5 nm) started to increase from an incubation time which is specific to each tested ligand. Indeed, the starting time for the size growth of HEWL aggregates was found to be 24 hrs for the resveratrol, 72 hrs for the HEWL samples containing the dopamine or nicotine, 96 hrs for

the tyrosol and 144 hrs in the presence of rutin. Conversely, it can be observed that at the end of the aggregation process, the dopamine, resveratrol and nicotine compounds generate HEWL aggregates which are smaller (17-24 nm) than those obtained in the presence of rutin and tyrosol (35-37 nm). Although our DLS measurements give rather qualitative information about the kinetics of HEWL aggregation, we nevertheless observed that each inhibitor exerts its inhibitory effects by reducing the production of amyloidogenic forms (oligomers and protofibrils) in favour of very small amorphous aggregates.

II.3. HEWL fibrillogenesis inhibition as monitored by Trp fluorescence

In our previous report (Dumoulin, Kumita, and Dobson 2006), we have shown that the dominating fluorophores Trp^{62} and Trp^{108} of HEWL, responsible for ~80 % of the total fluorescence emission of the protein, are effective probes of all conformational events occurring during the entire fibrillation process of HEWL. Given the aforementioned observations, we exploited the fluorescence characteristics of these Trp residues (maximum intensity (I_{max}) or fluorescence quantum yield (Q_f) and wavelength of the maximum intensity (λ_{max})) (Eftink and Ghiron 1976; Vivian and Callis 2001) to characterize the time dependency of the extent of lysozyme aggregation in the presence of each compound.

Fig **7** reports on the Trp fluorescence emission spectra of HEWL species generated by the dopamine, nicotine and tyrosol compounds (excitation at 295 nm) obtained at different incubation times. Compared to the spectrum of the monomeric HEWL (control sample), these Trp fluorescence spectra exhibit a significant decrease of their Trp fluorescence quantum yield (as given by the area under the spectra) with the incubation time whereas the wavelength of their maximum intensity, situated around 340±3 nm, does not change drastically. The same results were obtained for the other ligand-containing HEWL samples but the extent of the reduction of

Q_f is depending of the tested compound. Indeed, the amount of the reduction (the Q_f value of Trp observed for the monomeric lysozyme in the presence of each ligand at the initial time was taken as 100%) varies from 40% in the presence of tyrosol to ~65% in the presence of resveratrol. Given that the solvent-exposed Trp residues in proteins usually exhibit a decrease in I_{max} with a substantial red shift in λ_{max} (Eftink and Ghiron 1976; Vivian and Callis 2001), the observed quenching of the Trp fluorescence in the presence of each ligand would result from the intra- and/or inter-molecular interactions of the Trp microenvironment with neighbouring residues within the HEWL aggregates generated by each ligand (Nishimoto et al. 1998; Burley and Petsko 1986; Rholam, Scarlata, and Weber 1984).

Fig **8** exhibits the Trp fluorescence-monitored kinetics of HEWL aggregation which is characterized by distinct monotonic time decreases in the presence of each ligand. Linear regression analysis of these Trp fluorescence kinetics data gives the values of the rate constant (k_i) of the changes of Trp photophysical features, as listed in the table **6**. The analysis of these results allows us to deduce the following observations. Firstly, the time-dependent decrease of the Trp fluorescence quantum yield during the aggregation of HEWL exhibits two phases (Fig 8A,B) in the presence of dopamine and rutin (Group I) and three phases (Fig 8C,D,E) in the presence of tyrosol, resveratrol and nicotine (Group II). Qualitatively, this indicates that the compounds of each group produce different types of quenching interactions in the generated HEWL species. Indeed, the changes in the Trp photophysical features, produced by the rutin (1^{st} group) and by the resveratrol and nicotine (2^{nd} group), are most marked during the first phase ($[k_1/k_2]>1$) whereas those, induced by the dopamine (1^{st} group) and tyrosol (2^{nd} group), are most pronounced during the second phase ($[k_1/k_2]<1$). Moreover, the rate constant k_3 of the resveratrol and nicotine molecules (2^{nd} group) is 2-fold faster than that of the tyrosol compound. Secondly, the fastest changes in the fluorescence quenching of Trp are produced by the resveratrol during

the first and third phases (k_1=-0,606 h^{-1} and k_3=-0,276 h^{-1}) and by the tyrosol during the second phase (k_2=-0,374 h^{-1}). Conversely, the slowest changes in the Trp fluorescence quantum were observed for the tyrosol during the first and third phases (k_1=-0,065 h^{-1} and k_3=-0,123 h^{-1}) and for the resveratrol during the second phase (k_2=-0,040 h^{-1}). Thirdly, the rutin and nicotine molecules, producing parallel effects on the Trp fluorescence during the two first phases (k_1/k_2[nicotine]>k_1/k_2[rutin]>1), or the resveratrol and tyrosol compounds, exerting opposite effects on the Trp fluorescence during the same phases (k_1/k_2[resveratrol]>1>k_1/k_2[tyrosol]), exhibit a similar value for the product of their k_1 and k_2 rate constants ($k_1.k_2$[resveratrol]=$k_1.k_2$[tyrosol]=~0.040 and $k_1.k_2$[rutin]=$k_1.k_2$[nicotine]=~0.024). Qualitatively, this means that the Trp spectroscopic features undergo comparable effects by the compounds of each pair at the end of the time period corresponding to the two first phases of HEWL aggregation. Regardless of the exact nature of these distinguishing spectroscopic features of Trp, the kinetics of HEWL amyloid formation, monitored by the Trp fluorescence, displays kinetic parameters indicating that the Trp environments of HEWL undergo different modifications depending on both the chemical nature of compounds and the step at which these inhibitors interfere within the assembly process of HEWL.

III. Dose-dependent inhibition of HEWL fibril formation by natural compounds.

Generally, the effects of molecule inhibitors of protein self-assembly can vary depending on the conditions in which they are assessed such as the point(s) at which these inhibitors intercede within the assembly process or the protein/inhibitor molar ratio. Therefore, to complete the analysis of inhibition potency compounds done in the previous sections for the drug-to-protein molar ratio of 1:1 at different phases of HEWL aggregation, we have investigated in this part the

concentration-dependence of inhibition of fibril formation by each compound using the same biophysical methods.

III.1. Concentration dependent effects of Inhibitors as assessed by ThT fluorescence.

To investigate the dependence of concentration levels of each ligand on the HEWL fibril generation under our aggregation conditions (see material and methods), we performed several dose-dependency experiments at different steps along the self-assembly pathway of HEWL. Then, their ability to reduce dose-dependently HEWL fibril formation was quantitatively assessed via comparison of experimental plateau ThT fluorescence values of samples containing the ligands to that of the control sample (taken as 100%).

Fig **9A** exhibits the patterns of dose-dependent inhibition of fibril formation by each compound obtained for different drug-to-protein molar ratios after completion of the stationary phase (incubation of 264 hr). As shown, the inhibitory effect of each compound was increased as the drug-to-protein molar ratio raised from 10^{-4} to 4, indicating that all the compounds clearly retarded the formation of HEWL oligomers/fibrils in a concentration-dependent manner. The highest anti-amyloidogenic inhibitory effect of each ligand was observed at a drug-to-protein molar ratio higher than 1:1 (>~95% decrease of ThT fluorescence relative to that of HEWL alone). The values of inhibitory concentration (IC50) of rutin, dopamine, nicotine, resveratrol and tyrosol, required to inhibit the formation of HEWL fibrils to 50% of the control value, were derived from the sigmoidal curve fitting of the experimental data (Fig **9A**). The analysis of these values, summarized in the table **7**, allows us to deduce the following observations. Firstly, the best fit of the data was obtained by using the two-site competitive binding model, indicating that each compound exhibits two binding sites with distinct affinities ($IC50_1$ and $IC50_2$). Secondly, the $IC50_2$ (high affinity) value of rutin is approximately 2-fold lower than that of the other ligands whereas the $IC50_1$ (low affinity) value of resveratrol is ~4-fold lower than that of rutin,

tyrosol and dopamine and ~8-fold-lower than that of nicotine. Thirdly, all the tested ligands exhibit different values for the parameter P, which represents the fraction of the site 1. Indeed, the tyrosol rather binds to the low affinity site ($IC50_1$, P>50%) whereas the nicotine, rutin and dopamine molecules preferably bind to the high affinity site ($IC50_2$, P<50%). This contrasts with the resveratrol which exhibits close values for the both half-maximal inhibitions ($IC50_1$=~8x$IC50_2$) and binds to the two sites with the same probability (P=~50%).

To gain more insights with regard to the equilibrium phase in which the inhibitors are effective, dose-dependency experiments were performed at certain time points of the polymerization and nucleation phases. The results (data not shown), obtained for the 96 hrs and 144 hrs incubations (polymerization phase) of ligand-containing HEWL samples, indicate that all the compounds dose-dependently inhibited the polymerization phase and also exhibit sigmoidal dose–response curves described by the two-site competitive binding model as shown for the end point of the stationary phase (Fig 9). The analysis of parameters (IC50 and P), derived from these dose-response curves, reveals the following: *i*)-the $IC50_1$ values for inhibition of HEWL polymerization were approximately similar to those presented in the table **7, *ii*)**-the P values are quite different from those obtained for the stationary phases and ***iii***)-the $IC50_2$ values of the 96 hrs incubation, unlike those of the 144 hrs incubation, are ~10-fold higher than that obtained for the equilibrium phase. For the nucleation phase (incubation of 48h and 72h), the compounds exhibit also a sigmoidal dose–response curve but it is characterized by the one-site competitive binding model. For illustration, we give the pattern of dose-dependent inhibition of the 48 hours aggregation reaction of HEWL by each ligand at different drug-to-protein molar ratios (Fig. **9B**). Interestingly, the IC50 values, deduced from these dose-response curves, are roughly similar to those obtained for the low affinity-binding site ($IC50_1$) of the stationary and polymerization phases of HEWL kinetics.

Conclusion

In the present study, we conducted a series of biophysical experiments to explore the amyloid fibril inhibition effect of natural compounds from different groups (polyphenols, flavanol, alkaloid and catecholamine) using the well-characterized protein system hen egg white lysozyme. Taken together, the experimental data above revealed that all the used compounds are capable to inhibit amyloid fibril formation in a concentration dependent manner. In particular DLS and AFM imaging confirmed the reduction of the size/fibrils when the protein was incubated in presence if one of these compounds. This indicate that all these small molecules reduce not only the size of the formed species but also the fibril length and number. Importantly, these natural compounds are also capable to prevent the structural transition from the native α–helix rich HEWL conformer to amyloidogenic β–sheet rich species, affecting the process of fibril formation. Despite the differences of the used compounds, this work provides further insight into the effect of each compound on amyloid fibril formation of HEWL. Moreover, given that the structural features (local, secondary, oligomeric and fibrillar structures) observed in the presence of inhibitors have not been reported before for this amyloid system, we believe that the detailed approach established in the present work would be useful for a systematic investigation of anti-amyloid compounds targeting various stages of process of aggregation proteins.

Acknowledgments

This work was supported in part by funds from the Université Paris Diderot and the CNRS to ITODYS-UMR CNRS 7086 and from the Université de Versailles Saint-Quentin-en-Yvelines to the Laboratoire de Génétique et Biologie Cellulaire. Ali Chaari is a recipient of a doctoral fellowship from the French Ministry of Higher Education.

We thank Dr Ahmed HAOUZ (Responsable Plate-forme 6, Institut Pasteur, Paris, France) for his help in DLS experiments and analysis.

Competing interests

The authors have declared that no competing interests exist

References

Alam, Parvez, Sumit Kumar Chaturvedi, Mohammad Khursheed Siddiqi, Ravi Kant Rajpoot, Mohd Rehan Ajmal, Masihuz Zaman, and Rizwan Hasan Khan. 2016. “Vitamin K3 Inhibits Protein Aggregation: Implication in the Treatment of Amyloid Diseases.” *Scientific Reports* 6: 26759. https://doi.org/10.1038/srep26759.

Alam, Parvez, Khursheed Siddiqi, Sumit Kumar Chturvedi, and Rizwan Hasan Khan. 2017. “Protein Aggregation: From Background to Inhibition Strategies.” *International Journal of Biological Macromolecules* 103 (October): 208–19. https://doi.org/10.1016/j.ijbiomac.2017.05.048.

Amijee, Hozefa, Jill Madine, David A. Middleton, and Andrew J. Doig. 2009. “Inhibitors of Protein Aggregation and Toxicity.” *Biochemical Society Transactions* 37 (4): 692–96. https://doi.org/10.1042/BST0370692.

and, Yu Chen, and Mary D. Barkley*. 1998. “Toward Understanding Tryptophan Fluorescence in Proteins†.” https://doi.org/10.1021/BI980274N.

Baur, Joseph A., and David A. Sinclair. 2006. “Therapeutic Potential of Resveratrol: The in Vivo Evidence.” *Nature Reviews Drug Discovery* 5 (6): 493–506. https://doi.org/10.1038/nrd2060.

Bucciantini, Monica, Elisa Giannoni, Fabrizio Chiti, Fabiana Baroni, Lucia Formigli, Jesús Zurdo, Niccolò Taddei, Giampietro Ramponi, Christopher M. Dobson, and Massimo Stefani. 2002. “Inherent Toxicity of Aggregates Implies a Common Mechanism for Protein Misfolding Diseases.” *Nature* 416 (6880): 507–11. https://doi.org/10.1038/416507a.

Burley, S K, and G A Petsko. 1986. “Amino-Aromatic Interactions in Proteins.” *FEBS Letters* 203 (2): 139–43. http://www.ncbi.nlm.nih.gov/pubmed/3089835.

Byler, D. Michael, and Heino Susi. 1986. “Examination of the Secondary Structure of Proteins by Deconvolved FTIR Spectra.” *Biopolymers* 25 (3): 469–87. https://doi.org/10.1002/bip.360250307.

Cabaleiro-Lago, C., O. Szczepankiewicz, and S. Linse. 2012. “The Effect of Nanoparticles on Amyloid Aggregation Depends on the Protein Stability and Intrinsic Aggregation Rate.” *Langmuir* 28 (3): 1852–57. https://doi.org/10.1021/la203078w.

Cavalli, Andrea, Maria Laura Bolognesi, Anna Minarini, Michela Rosini, Vincenzo Tumiatti, Maurizio Recanatini, and Carlo Melchiorre. 2008. “Multi-Target-Directed Ligands To Combat Neurodegenerative Diseases.” *Journal of Medicinal Chemistry* 51 (3): 347–72. https://doi.org/10.1021/jm7009364.

Chaari, Ali, Christine Fahy, Alexandre Chevillot-Biraud, and Mohamed Rholam. 2015. “Insights into Kinetics of Agitation-Induced Aggregation of Hen Lysozyme under Heat and Acidic Conditions from Various Spectroscopic Methods.” Edited by Rizwan Hasan Khan. *PLOS ONE* 10 (11): e0142095. https://doi.org/10.1371/journal.pone.0142095.

Chamberlain, Aaron K., Cait E. MacPhee, Jesús Zurdo, Ludmilla A. Morozova-Roche, H. Allen O. Hill, Christopher M. Dobson, and Jason J. Davis. 2000. “Ultrastructural Organization of Amyloid Fibrils ByAtomic Force Microscopy.” *Biophysical Journal* 79 (6): 3282–93. https://doi.org/10.1016/S0006-3495(00)76560-X.

Chiti, Fabrizio, and Christopher M. Dobson. 2006. “Protein Misfolding, Functional Amyloid, and Human Disease.” *Annual Review of Biochemistry* 75 (1): 333–66. https://doi.org/10.1146/annurev.biochem.75.101304.123901.

DaSilva, Kevin A., James E. Shaw, and JoAnne McLaurin. 2010. “Amyloid-β Fibrillogenesis:

Structural Insight and Therapeutic Intervention." *Experimental Neurology* 223 (2): 311–21. https://doi.org/10.1016/j.expneurol.2009.08.032.

Dolphin, Gunnar T., Myriam Ouberai, Pascal Dumy, and Julian Garcia. 2007. "Designed Amyloid β Peptide Fibril—A Tool for High-Throughput Screening of Fibril Inhibitors." *ChemMedChem* 2 (11): 1613–23. https://doi.org/10.1002/cmdc.200700103.

Dumoulin, Mireille, Janet R. Kumita, and Christopher M. Dobson. 2006. "Normal and Aberrant Biological Self-Assembly: Insights from Studies of Human Lysozyme and Its Amyloidogenic Variants." *Accounts of Chemical Research* 39 (9): 603–10. https://doi.org/10.1021/ar050070g.

Eftink, M. R., and C. A. Ghiron. 1976. "Exposure of Tryptophanyl Residues in Proteins. Quantitative Determination by Fluorescence Quenching Studies." *Biochemistry* 15 (3): 672–80. https://doi.org/10.1021/bi00648a035.

Eftink, M R. 1991. "Fluorescence Techniques for Studying Protein Structure." *Methods of Biochemical Analysis* 35: 127–205. http://www.ncbi.nlm.nih.gov/pubmed/2002770.

Florent-Béchard, Sabrina, Cédric Desbène, Pierre Garcia, Ahmad Allouche, Ihsen Youssef, Marie-Christine Escanyé, Violette Koziel, et al. 2009. "The Essential Role of Lipids in Alzheimer's Disease." *Biochimie* 91 (6): 804–9. https://doi.org/10.1016/j.biochi.2009.03.004.

Galleano, Mónica, Sandra V. Verstraeten, Patricia I. Oteiza, and Cesar G. Fraga. 2010. "Antioxidant Actions of Flavonoids: Thermodynamic and Kinetic Analysis." *Archives of Biochemistry and Biophysics* 501 (1): 23–30. https://doi.org/10.1016/j.abb.2010.04.005.

Gazova, Zuzana, Katarina Siposova, Elena Kurin, Pavel Mučaji, and Milan Nagy. 2013. "Amyloid Aggregation of Lysozyme: The Synergy Study of Red Wine Polyphenols." *Proteins: Structure, Function, and Bioinformatics* 81 (6): 994–1004. https://doi.org/10.1002/prot.24250.

Gharibyan, Anna L., Vladimir Zamotin, Kiran Yanamandra, Olesya S. Moskaleva, Boris A. Margulis, Irina A. Kostanyan, and Ludmilla A. Morozova-Roche. 2007. "Lysozyme Amyloid Oligomers and Fibrils Induce Cellular Death via Different Apoptotic/Necrotic Pathways." *Journal of Molecular Biology* 365 (5): 1337–49. https://doi.org/10.1016/j.jmb.2006.10.101.

Giovanni, Saviana Di, Simona Eleuteri, Katerina E Paleologou, Guowei Yin, Markus Zweckstetter, Pierre-Alain Carrupt, and Hilal A Lashuel. 2010. "Entacapone and Tolcapone, Two Catechol O-Methyltransferase Inhibitors, Block Fibril Formation of Alpha-Synuclein and Beta-Amyloid and Protect against Amyloid-Induced Toxicity." *The Journal of Biological Chemistry* 285 (20): 14941–54. https://doi.org/10.1074/jbc.M109.080390.

Grondelle, Wilmar van, Carmen López Iglesias, Elisenda Coll, Franck Artzner, Maïté Paternostre, Frédéric Lacombe, Merce Cardus, et al. 2007. "Spontaneous Fibrillation of the Native Neuropeptide Hormone Somatostatin-14." *Journal of Structural Biology* 160 (2): 211–23. https://doi.org/10.1016/j.jsb.2007.08.006.

Grudzielanek, Stefan, Aleksandra Velkova, Anuj Shukla, Vytautas Smirnovas, Marianna Tatarek-Nossol, Heinz Rehage, Aphrodite Kapurniotu, and Roland Winter. 2007. "Cytotoxicity of Insulin within Its Self-Assembly and Amyloidogenic Pathways." *Journal of Molecular Biology* 370 (2): 372–84. https://doi.org/10.1016/J.JMB.2007.04.053.

Hartl, F. Ulrich. 2017. "Protein Misfolding Diseases." *Annual Review of Biochemistry* 86 (1): 21–26. https://doi.org/10.1146/annurev-biochem-061516-044518.

Hutt, Darren M, Evan T Powers, and William E Balch. 2009. "The Proteostasis Boundary in Misfolding Diseases of Membrane Traffic." *FEBS Letters* 583 (16): 2639–46.

http://www.ncbi.nlm.nih.gov/pubmed/19708088.
Ishtikhar, Mohd, Salman Sadullah Usmani, Nuzhat Gull, Gamal Badr, Mohamed H. Mahmoud, and Rizwan Hasan Khan. 2015. “Inhibitory Effect of Copper Nanoparticles on Rosin Modified Surfactant Induced Aggregation of Lysozyme.” *International Journal of Biological Macromolecules* 78 (July): 379–88. https://doi.org/10.1016/j.ijbiomac.2015.03.069.
Jayaraman, Murali, Ravindra Kodali, Bankanidhi Sahoo, Ashwani K. Thakur, Anand Mayasundari, Rakesh Mishra, Cynthia B. Peterson, and Ronald Wetzel. 2012. “Slow Amyloid Nucleation via α-Helix-Rich Oligomeric Intermediates in Short Polyglutamine-Containing Huntingtin Fragments.” *Journal of Molecular Biology* 415 (5): 881–99. https://doi.org/10.1016/j.jmb.2011.12.010.
Jean, Létitia, Chiu Fan Lee, Michael Shaw, and David J. Vaux. 2008. “Structural Elements Regulating Amyloidogenesis: A Cholinesterase Model System.” Edited by Suzannah Rutherford. *PLoS ONE* 3 (3): e1834. https://doi.org/10.1371/journal.pone.0001834.
Jiménez, José L, Glenys Tennent, Mark Pepys, and Helen R Saibil. 2001. “Structural Diversity of Ex Vivo Amyloid Fibrils Studied by Cryo-Electron Microscopy.” *Journal of Molecular Biology* 311 (2): 241–47. https://doi.org/10.1006/jmbi.2001.4863.
Kayed, R., Elizabeth Head, Jennifer L Thompson, Theresa M McIntire, Saskia C Milton, Carl W Cotman, and Charles G Glabe. 2003. “Common Structure of Soluble Amyloid Oligomers Implies Common Mechanism of Pathogenesis.” *Science* 300 (5618): 486–89. https://doi.org/10.1126/science.1079469.
Khan, Javed M., Sumit K. Chaturvedi, Shah K. Rahman, Mohd. Ishtikhar, Atiyatul Qadeer, Ejaz Ahmad, and Rizwan H. Khan. 2014. “Protonation Favors Aggregation of Lysozyme with SDS.” *Soft Matter* 10 (15): 2591. https://doi.org/10.1039/c3sm52435c.
Khan, Mohsin Vahid, Gulam Rabbani, Mohd Ishtikhar, Shariqua Khan, Gajender Saini, and Rizwan Hasan Khan. 2015. “Non-Fluorinated Cosolvents: A Potent Amorphous Aggregate Inducer of Metalloproteinase-Conalbumin (Ovotransferrin).” *International Journal of Biological Macromolecules* 78 (July): 417–28. https://doi.org/10.1016/j.ijbiomac.2015.04.021.
Krimm, Samuel, and Jagdeesh Bandekar. 1986. “Vibrational Spectroscopy and Conformation of Peptides, Polypeptides, and Proteins.” *Advances in Protein Chemistry* 38 (January): 181–364. https://doi.org/10.1016/S0065-3233(08)60528-8.
Kumar, Jitendra, Risa Namsechi, and Valerie L. Sim. 2015. “Structure-Based Peptide Design to Modulate Amyloid Beta Aggregation and Reduce Cytotoxicity.” Edited by Jie Zheng. *PLOS ONE* 10 (6): e0129087. https://doi.org/10.1371/journal.pone.0129087.
Lee, S., Kenneth Carson, Allison Rice-Ficht, and Theresa Good. 2005. “Hsp20, a Novel -Crystallin, Prevents A Fibril Formation and Toxicity.” *Protein Science* 14 (3): 593–601. https://doi.org/10.1110/ps.041020705.
Legleiter, Justin, Dan L Czilli, Bruce Gitter, Ronald B DeMattos, David M Holtzman, and Tomasz Kowalewski. 2004. “Effect of Different Anti-Abeta Antibodies on Abeta Fibrillogenesis as Assessed by Atomic Force Microscopy.” *Journal of Molecular Biology* 335 (4): 997–1006. http://www.ncbi.nlm.nih.gov/pubmed/14698294.
Leong, Su Ling, Roberto Cappai, Kevin Jeffrey Barnham, and Chi Le Lan Pham. 2009. “Modulation of α-Synuclein Aggregation by Dopamine: A Review.” *Neurochemical Research* 34 (10): 1838–46. https://doi.org/10.1007/s11064-009-9986-8.
Levine, Harry. 2008. “Thioflavine T Interaction with Synthetic Alzheimer’s Disease β-Amyloid Peptides: Detection of Amyloid Aggregation in Solution.” *Protein Science* 2 (3): 404–10.

https://doi.org/10.1002/pro.5560020312.
Lindner, Ariel B., and Alice Demarez. 2009. “Protein Aggregation as a Paradigm of Aging.” *Biochimica et Biophysica Acta (BBA) - General Subjects* 1790 (10): 980–96. https://doi.org/10.1016/j.bbagen.2009.06.005.
Liu, Quan, Fang Xie, Raj Rolston, Paula I Moreira, Akihiko Nunomura, Xiongwei Zhu, Mark A Smith, and George Perry. 2007. “Prevention and Treatment of Alzheimer Disease and Aging: Antioxidants.” *Mini Reviews in Medicinal Chemistry* 7 (2): 171–80. http://www.ncbi.nlm.nih.gov/pubmed/17305591.
Liu, R, R Su, M Liang, R Huang, M Wang, W Qi, and Z He. 2012. “Physicochemical Strategies for Inhibition of Amyloid Fibril Formation: An Overview of Recent Advances.” *Current Medicinal Chemistry* 19 (24): 4157–74. http://www.ncbi.nlm.nih.gov/pubmed/22830338.
Lomakin, A, D S Chung, G B Benedek, D A Kirschner, D B Teplow, Tuomas P. J. Knowles, Sara Linse, and Christopher M. Dobson. 1996. “On the Nucleation and Growth of Amyloid Beta-Protein Fibrils: Detection of Nuclei and Quantitation of Rate Constants.” *Proceedings of the National Academy of Sciences of the United States of America* 93 (3): 1125–29. https://doi.org/10.1073/pnas.93.3.1125.
Masuda, Masami, Nobuyuki Suzuki, Sayuri Taniguchi, Takayuki Oikawa, Takashi Nonaka, Takeshi Iwatsubo, Shin-ichi Hisanaga, Michel Goedert, and Masato Hasegawa. 2006. “Small Molecule Inhibitors of α-Synuclein Filament Assembly †.” *Biochemistry* 45 (19): 6085–94. https://doi.org/10.1021/bi0600749.
Moran, Valentina Echeverria. 2013. “Brain Effects of Nicotine and Derived Compounds.” *Frontiers in Pharmacology* 4. https://doi.org/10.3389/FPHAR.2013.00060.
Morris, Aimee M., Murielle A. Watzky, and Richard G. Finke. 2009. “Protein Aggregation Kinetics, Mechanism, and Curve-Fitting: A Review of the Literature.” *Biochimica et Biophysica Acta (BBA) - Proteins and Proteomics* 1794 (3): 375–97. https://doi.org/10.1016/j.bbapap.2008.10.016.
Nishimoto, Etsuko, Shoji Yamashita, Arthur G. Szabo, and Taiji Imoto. 1998. “Internal Motion of Lysozyme Studied by Time-Resolved Fluorescence Depolarization of Tryptophan Residues.” *Biochemistry* 37 (16): 5599–5607. https://doi.org/10.1021/bi9718651.
Ono, Kenjiro, Tsuyoshi Hamaguchi, Hironobu Naiki, and Masahito Yamada. 2006. “Anti-Amyloidogenic Effects of Antioxidants: Implications for the Prevention and Therapeutics of Alzheimer’s Disease.” *Biochimica et Biophysica Acta (BBA) - Molecular Basis of Disease* 1762 (6): 575–86. https://doi.org/10.1016/j.bbadis.2006.03.002.
Porat, Yair, Adel Abramowitz, and Ehud Gazit. 2006. “Inhibition of Amyloid Fibril Formation by Polyphenols: Structural Similarity and Aromatic Interactions as a Common Inhibition Mechanism.” *Chemical Biology <html_ent Glyph="@amp;" Ascii="&"/> Drug Design* 67 (1): 27–37. https://doi.org/10.1111/j.1747-0285.2005.00318.x.
Raccosta, Samuele, Vincenzo Martorana, and Mauro Manno. 2012. “Thermodynamic versus Conformational Metastability in Fibril-Forming Lysozyme Solutions.” *The Journal of Physical Chemistry B* 116 (40): 12078–87. https://doi.org/10.1021/jp303430g.
Rholam, Mohamed, Suzanne Scarlata, and Gregorio Weber. 1984. “Frictional Resistance to the Local Rotations of Fluorophores in Proteins.” *Biochemistry* 23 (26): 6793–96. https://doi.org/10.1021/bi00321a079.
Ruzafa, David, Bertrand Morel, Lorena Varela, Ana I. Azuaga, and Francisco Conejero-Lara. 2012. “Characterization of Oligomers of Heterogeneous Size as Precursors of Amyloid Fibril Nucleation of an SH3 Domain: An Experimental Kinetics Study.” Edited by Human Rezaei. *PLoS ONE* 7 (11): e49690. https://doi.org/10.1371/journal.pone.0049690.

Santhoshkumar, Puttur, and Krishna K. Sharma. 2004. “Inhibition of Amyloid Fibrillogenesis and Toxicity by a Peptide Chaperone.” *Molecular and Cellular Biochemistry* 267 (1/2): 147–55. https://doi.org/10.1023/B:MCBI.0000049373.15558.b8.

Scarpini, Elio, Daniela Galimberti, and Laura Ghezzi. 2013. “Disease-Modifying Drugs in Alzheimer's Disease.” *Drug Design, Development and Therapy* 7 (December): 1471. https://doi.org/10.2147/DDDT.S41431.

Selkoe, Dennis J. 2004. “Cell Biology of Protein Misfolding: The Examples of Alzheimer’s and Parkinson’s Diseases.” *Nature Cell Biology* 6 (11): 1054–61. https://doi.org/10.1038/ncb1104-1054.

Siddiqi, Mohammad Khursheed, Parvez Alam, Sumit Kumar Chaturvedi, Yasser E Shahein, and Rizwan Hasan Khan. 2017. “Mechanisms of Protein Aggregation and Inhibition.” *Frontiers in Bioscience (Elite Edition)* 9: 1–20. http://www.ncbi.nlm.nih.gov/pubmed/27814585.

Stefani, Massimo, and Stefania Rigacci. 2013. “Protein Folding and Aggregation into Amyloid: The Interference by Natural Phenolic Compounds.” *International Journal of Molecular Sciences* 14 (6): 12411–57. https://doi.org/10.3390/ijms140612411.

Surewicz, Witold K., and Henry H. Mantsch. 1988. “New Insight into Protein Secondary Structure from Resolution-Enhanced Infrared Spectra.” *Biochimica et Biophysica Acta (BBA) - Protein Structure and Molecular Enzymology* 952 (January): 115–30. https://doi.org/10.1016/0167-4838(88)90107-0.

Swaminathan, Rajaram, Vijay Kumar Ravi, Satish Kumar, Mattaparthi Venkata Satish Kumar, and Nividh Chandra. 2011. “Lysozyme.” In *Advances in Protein Chemistry and Structural Biology*, 84:63–111. https://doi.org/10.1016/B978-0-12-386483-3.00003-3.

Takeuchi, Ken, Yoichi Nakatani, Osamu Hisatomi, Ken Takeuchi, Yoichi Nakatani, and Osamu Hisatomi. 2014. “Accuracy of Protein Size Estimates Based on Light Scattering Measurements.” *Open Journal of Biophysics* 04 (02): 83–91. https://doi.org/10.4236/ojbiphy.2014.42009.

Uversky, Vladimir N., and Anthony L. Fink. 2004. “Conformational Constraints for Amyloid Fibrillation: The Importance of Being Unfolded.” *Biochimica et Biophysica Acta (BBA) - Proteins and Proteomics* 1698 (2): 131–53. https://doi.org/10.1016/j.bbapap.2003.12.008.

Vivian, James T., and Patrik R. Callis. 2001. “Mechanisms of Tryptophan Fluorescence Shifts in Proteins.” *Biophysical Journal* 80 (5): 2093–2109. https://doi.org/10.1016/S0006-3495(01)76183-8.

Figure Legends

Figure 1. Chemical structure of natural compounds tested as inhibitors of HEWL fibril formation.

Figure 2. Morphological characterization of HEWL aggregates by AFM. The AFM images of an aliquot from the solutions were obtained at the 264 hour incubation of HEWL alone (**A**) and in the presence of an equimolar concentration of resveratrol (**B**), tyrosol (**C**), rutin (**D**), nicotine (**E**) and dopamine (**F**). AFM images of HEWL solutions were registered at the concentration of 10 μM.

Figure 3. Secondary structural characterization of lysozyme species by FTIR. The ATR-FTIR spectra were registered at the 264 hour incubation of HEWL solutions with the presence of an equimolar concentration of nicotine (**A**) tyrosol (**B**), rutin (**C**), dopamine (**D**) and resveratrol (**E**). Measurements, obtained from three independent experiments, were performed for different protein concentrations. The arrows point to the maximum intensities.

Figure 4. Inhibition of amyloid fibrillogenesis kinetics of HEWL followed by ThT fluorescence. The data represent the temporal evolution of the quantum yield of ThT fluorescence during the aggregation process of HEWL in the presence of each compound at a concentration equimolar to HEWL monomer (1.4 mM). The values of the fluorescence quantum yield of ThT are the mean of three independent measurements, each performed in quadruplicate. HEWL solutions were subjected to this analysis at the concentration of 10 μM.

Figure 5. Dynamic light scattering during HEWL fibrillization. Size distribution by mass for HEWL alone (**A**) and in the presence of dopamine (**B**) resveratrol (**C**), nicotine (**D**), tyrosol (**E**) and rutin (**F**) at a concentration equimolar to HEWL monomer (1.4 mM) for an incubation of 264 hrs. Measurements of HEWL solutions, performed in triplicate, were done at the protein concentration of 1 mg/ml.

Figure 6. Inhibition of amyloid fibrillogenesis kinetics of HEWL monitored by DLS. The data represent the temporal evolution of the average hydrodynamic radius <Rh> of HEWL species formed during the aggregation process. The values of <Rh> were deduced from the DLS graphs as shown in the figure **6**.

Figure 7. Trp fluorescence spectra of HEWL species recorded during the aggregation. The Trp emission spectra (excitation at 295 nm) of HEWL species, generated by dopamine (**A**) and nicotine (B) and tyrosol (C) at a concentration equimolar to HEWL monomer (1.4 mM), are the mean of four independent experiments, each performed in quadruplicate. Fluorescence measurements of HEWL solutions, at different incubation times, were acquired at the protein concentration of 1 mg/ml.

Figure 8. Inhibition of the aggregation kinetics of HEWL monitored by Trp fluorescence. The data represent the temporal evolution of the Trp fluorescence quantum yield of HEWL species formed during the aggregation process in the presence of resveratrol (A), nicotine (B), tyrosol (C), rutin (D) and dopamine (E) at a concentration equimolar to HEWL monomer (1.4 mM). The values of the Trp fluorescence quantum yield are given by the area under the emission

spectra as shown in the figure **8**. The line of best fit through the experimental data points was obtained by fitting the data with a linear function.

Figure 9. Aggregation of lysozyme observed at increasing concentration of compounds by ThT assay. The inhibiting ability of each ligand was quantified by fluorescence quantum yield, which was normalized to the control in the absence of compounds (100%). The single experiment was performed in triplicates. The error bars represent the average deviation for repeated measurements of three separate samples. The curves were obtained by fitting of the average values by non-linear least-square method.

A: After completion of the stationary phase (incubation of 264 hr).

B: After the lag phase (48 hours aggregation reaction).

Table 1. Size distribution of HEWL species (%) generated by each compound at the end of the protein aggregation process (incubation of 264 hours).

	L<15 nm	**15 nm<L<30 nm**	**L>30 nm**
HEWL + Nicotine	***88.6***	**14.4**	
HEWL + Tyrosol	**46.9**	**33.9**	**19.3**
HEWL + Dopamine	**27.0**	**59.2**	**13.8**
HEWL + Rutin	**23.1**	**59.1**	**17.8**
HEWL + Resveratrol	**14.0**	***70,3***	**15.7**

Table 2. Secondary-structure contents of HEWL species (%) generated by each compound at the end of the protein aggregation process (incubation of 264 hours).

	α-helix	β-sheet	Loops/turns	random coil
HEWL (264 hrs)	**19.0**	**71.0**	**11.0**	
HEWL + Dopamine	31.0	42.0	12.0	15.0
HEWL + Rutin	33.0	43.0	24.0	
HEWL + Resveratrol	42.0	34,0	24.0	
HEWL + Tyrosol	47.0	34.0	18.0	
HEWL + Nicotine	50.0	37.0	13.0	
HEWL (0 hrs)	**50.0**	**29.0**	**21.0**	

The proportions of each secondary structure have been calculated from the ATR-FTIR spectra shown in Fig. 3 by deconvolution and curve fitting of the Amide I band according to [**20**]

Table 3. Kinetics parameters of HEWL aggregation in the presence of each compound as determined by fitting of the ThT fluorescence curve shown in Fig 2

	$t_{0.5}$ (h)	$\tau = 1/k$ (h)	lag time (h)
HEWL + Tyrosol	143.8	32.6	78.6
HEWL + Rutin	166.9	34.7	97.5
HEWL + Nicotine	124.8	34.7	55.4
HEWL	**139.4**	**36.8**	**65.8**
HEWL + Resveratrol	173.6	45.2	83.2
HEWL + Dopamine	146.7	55.6	35.5

Table 4. Hydrodynamic radii of HEWL species generated by each compound at the end of the protein incubation process (incubation of 264 hours).

	$\langle R_h \rangle_M$ (nm)	$\langle R_h \rangle_m$ (nm)
HEWL (264 hrs)		**144.7**
HEWL + Dopamine	16.7 (87.0%)	116.1 (13.0%)
HEWL + Resveratrol	20.3 (88.0%)	122.9 (12.0%)
HEWL + Nicotine	23.8 (87.0%)	161.6 (13.0%)
HEWL + Rutin	34.7 (89.0%)	154.0 (11.0%)
HEWL + Tyrosol	36.6 (90.0%)	168.7 (10.0%)
HEWL (0 hrs)	**1.4**	

$\langle R_h \rangle_M$ and $\langle R_h \rangle_m$ correspond to the hydrodynamic radius obtained for the major (M) and minor (m) populations of HEWL species generated by each compound, respectively. The values in parenthesis correspond to the contribution of each particle population to the total DLS signal

Table 5. Hydrodynamic radius and percentage of HEWL species generated by each compound at some time points of the aggregation process of HEWL

	$\langle R_h \rangle_M$ (nm)				$\langle R_h \rangle_m$ (nm)			
	48 h	**72 h**	**96 h**	**144 h**	**48 h**	**72 h**	**96 h**	**144 h**
HEWL alone	**22,4** (95,6%)	**38,2** (99,6%)	**66,5** (100%)	**117,0** (100%)	**128,0** (4,4%)	**135,6** (0,4%)		
Nicotine	**1,6** (99,9%)	**1,6** (99,3%)	**6,7** (89,4%)	**13,7** (98,0%)	**14,9** (0,1%)	**10,4** (0,4%)	**34,2** (10,6%)	**11,5** (2,0%)
Rutin	**1,4** (99,2%)	**1,6** (99,2%)	**6,3** (97,6%)	**14,2** (88,6%)	**16,4** (0,7%)	**21,4** (0,8%)	**58,0** (2,4%)	**67,1** (11,4%)
Dopamine	**1,6** (99,7%)	**2,0** (98,4%)	**3,3** (92,1%)	**10,7** (98,6%)	**31,5** (0,3%)	**32,5** (1,6%)	**22,1** (7,7%)	**122,4** (1,4%)
Resveratrol	**2,1** (98,8%)	**1,7** (99,9%)	**6,9** (96,9%)	**14,2** (97,0%)	**29,0** (1,2%)	**15,2** (0,1%)	**73,6** (3,1%)	**109,3** (3,0%)
Tyrosol	**2,2** (97,1%)	**1,6** (99,0%)	**4,0** (96,9%)	**16,7** (92,7%)	**25,8** (2,8%)	**15,2** (0,7%)	**31,4** (3,0%)	**61,9** (7,3%)

$\langle R_h \rangle_M$ and $\langle R_h \rangle_m$ correspond to the hydrodynamic radius obtained for the major (M) and minor (m) populations of HEWL species generated by each compound, respectively. The values in parenthesis correspond to the contribution of each particle population to the total DLS signal.

Table 6. Rate constants (k_i) of Trp fluorescence changes during the aggregation of HEWL in the presence of each compound

	k_1 (h^{-1})	k_2 (h^{-1})	k_3 (h^{-1})
HEWL +Dopamine	-0,167	**-0,309**	
HEWL +Rutin	**-0,362**	-0,110	
HEWL +Tyrosol	-0,065	**-0,374**	-0,123
HEWL +Nicotine	**-0,508**	-0,079	-0,214
HEWL +Resveratrol	**-0,606**	-0,040	-0,276

Table 7. the aggregation of HEWL in the presence of each compound

	$10^4.IC50_1$ (M)	$10^6.IC50_2$ (M)	P (%)
HEWL +Rutin	1.17	1.41	***26.0***
HEWL +Dopamine	1.02	2.74	***29.0***
HEWL +Nicotine	2.58	2.66	***29.0***
HEWL +Resveratrol	0.31	2.52	***51.0***
HEWL +Tyrosol	1.32	2.59	***70.0***

Figure 1.

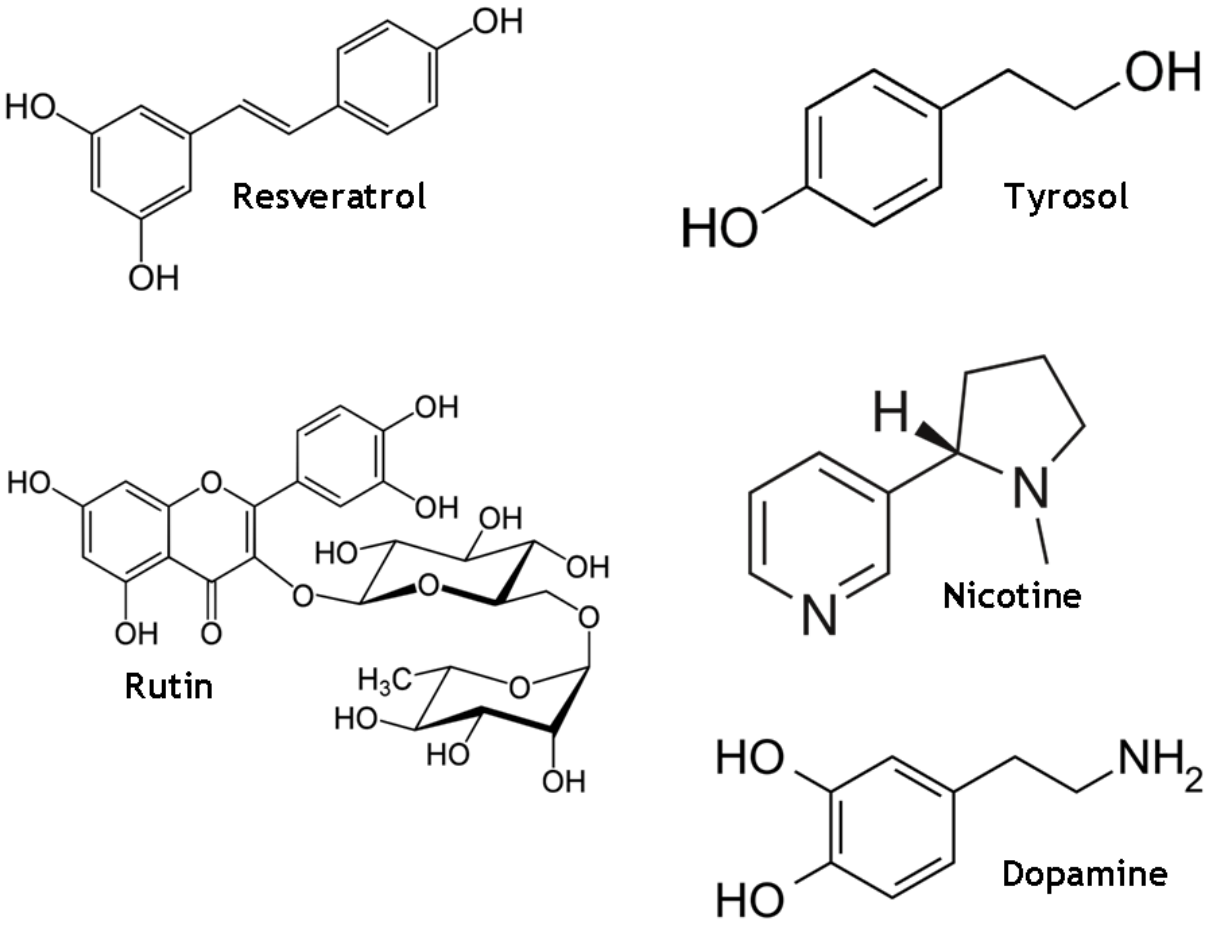
OH
HO
Resveratrol
OH
HO
Tyrosol
OH
H
N
N
Nicotine
HO
O
OH
OH
OH
HO
O
OH
O
OH
O
Rutin
H3C
O
HO
HO
OH
HO
NH2
HO
Dopamine

Figure 2.

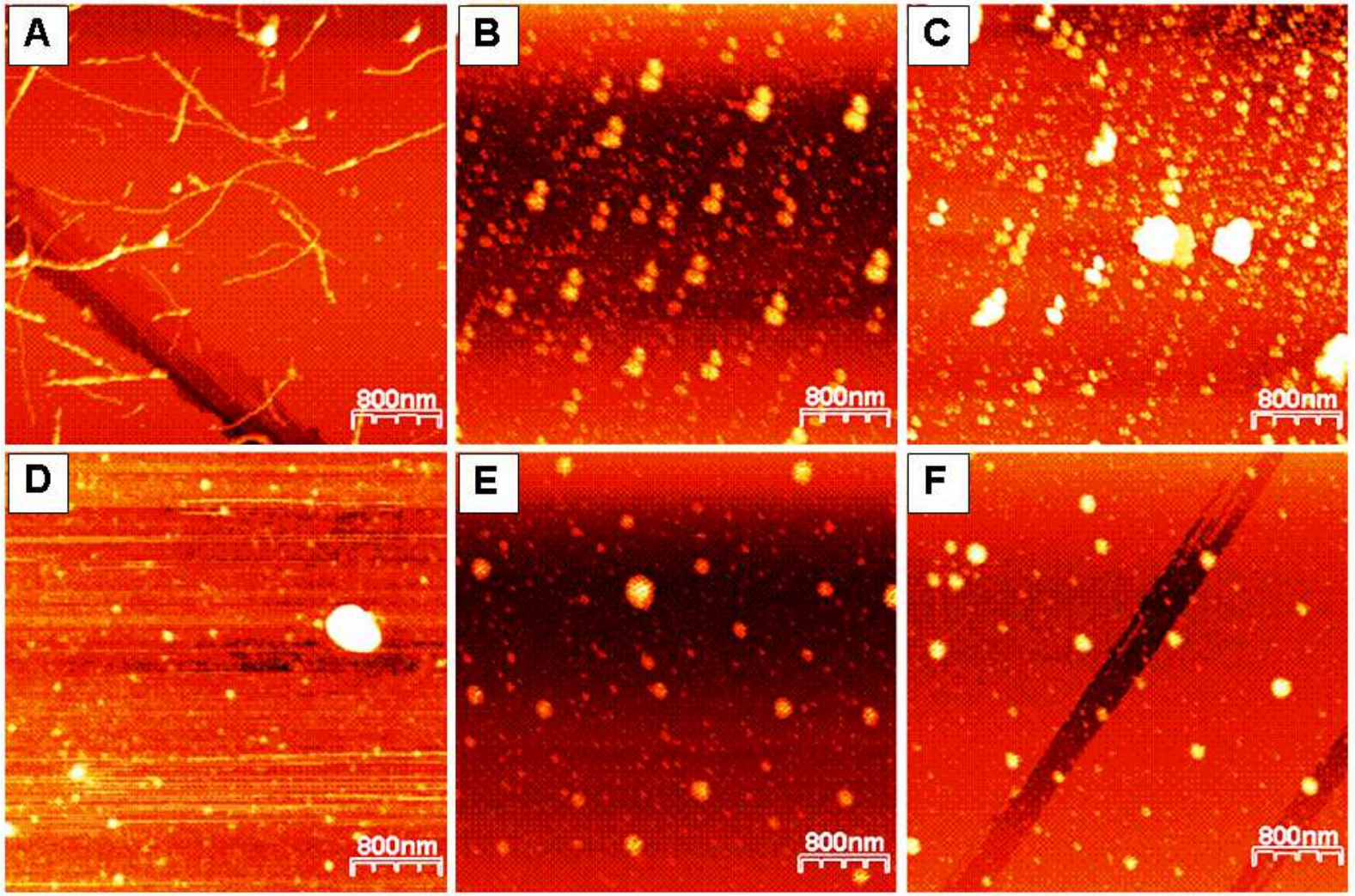

Figure 3..

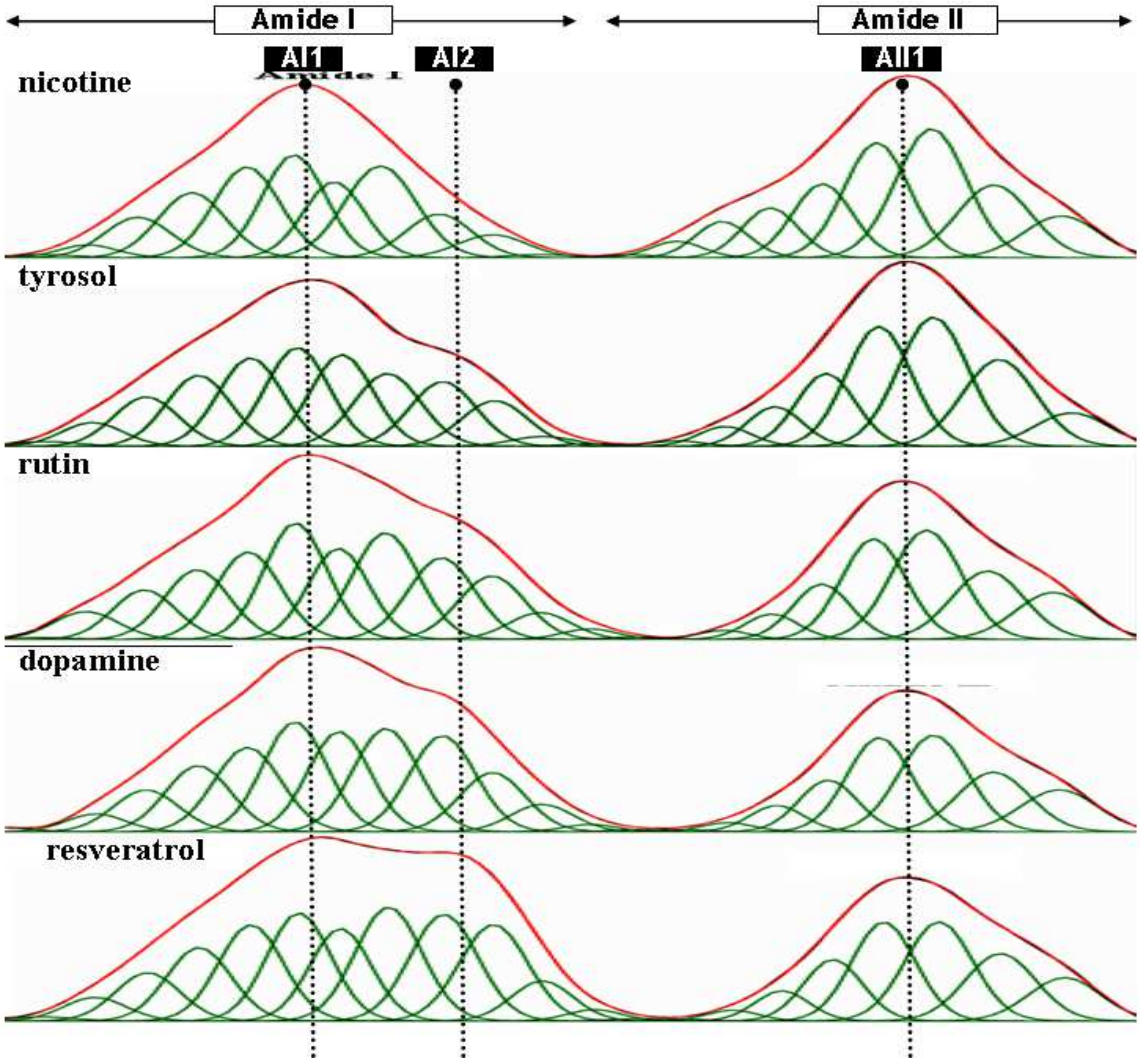
Amide I
Amide II
AI1
AI2
AII1
nicotine
tyrosol
rutin
dopamine
resveratrol

Figure 4.

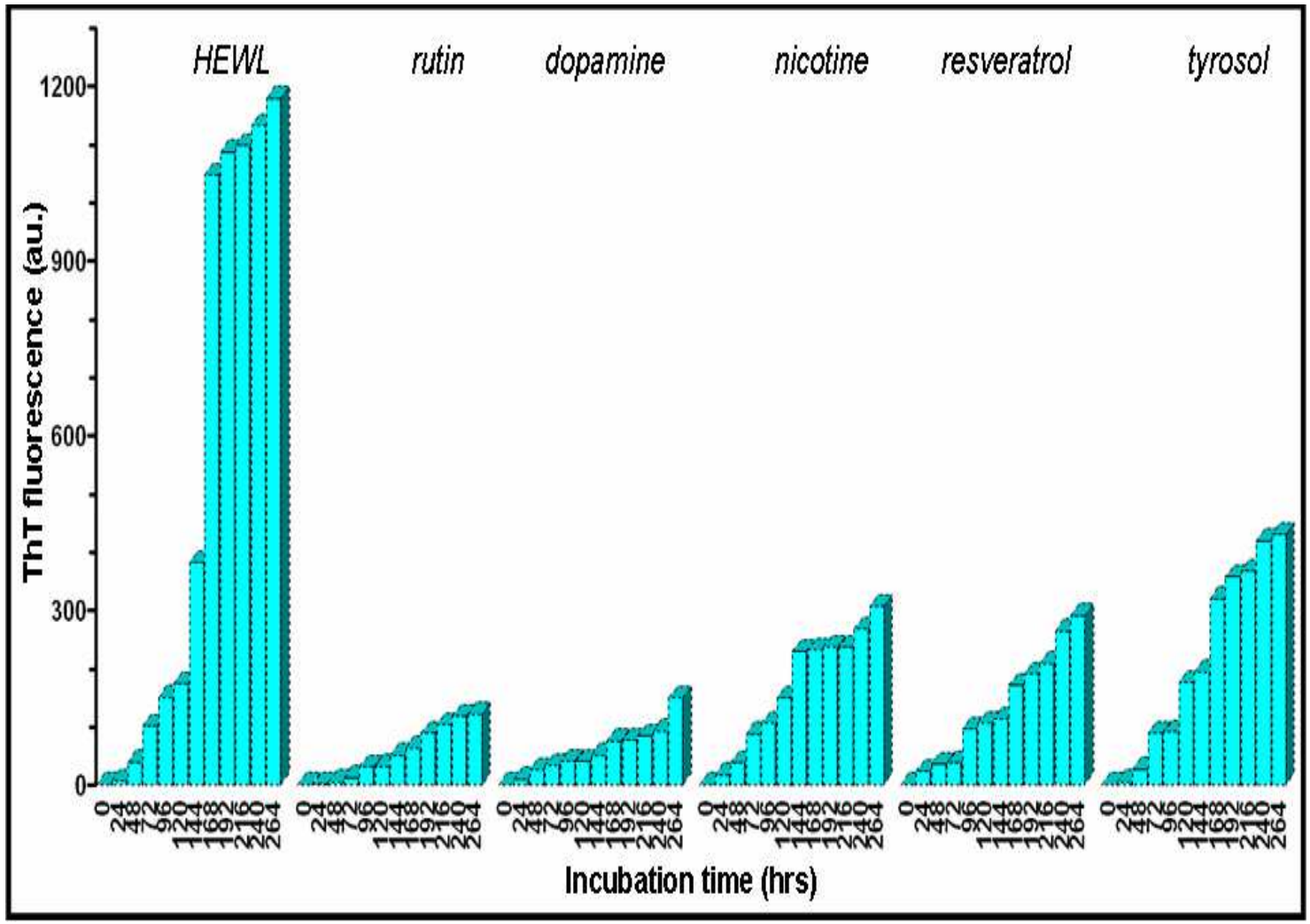
HEWL
rutin
dopamine
nicotine
resveratrol
tyrosol
ThT fluorescence (au.)
0
300
600
900
1200
Incubation time (hrs)

Figure 5.

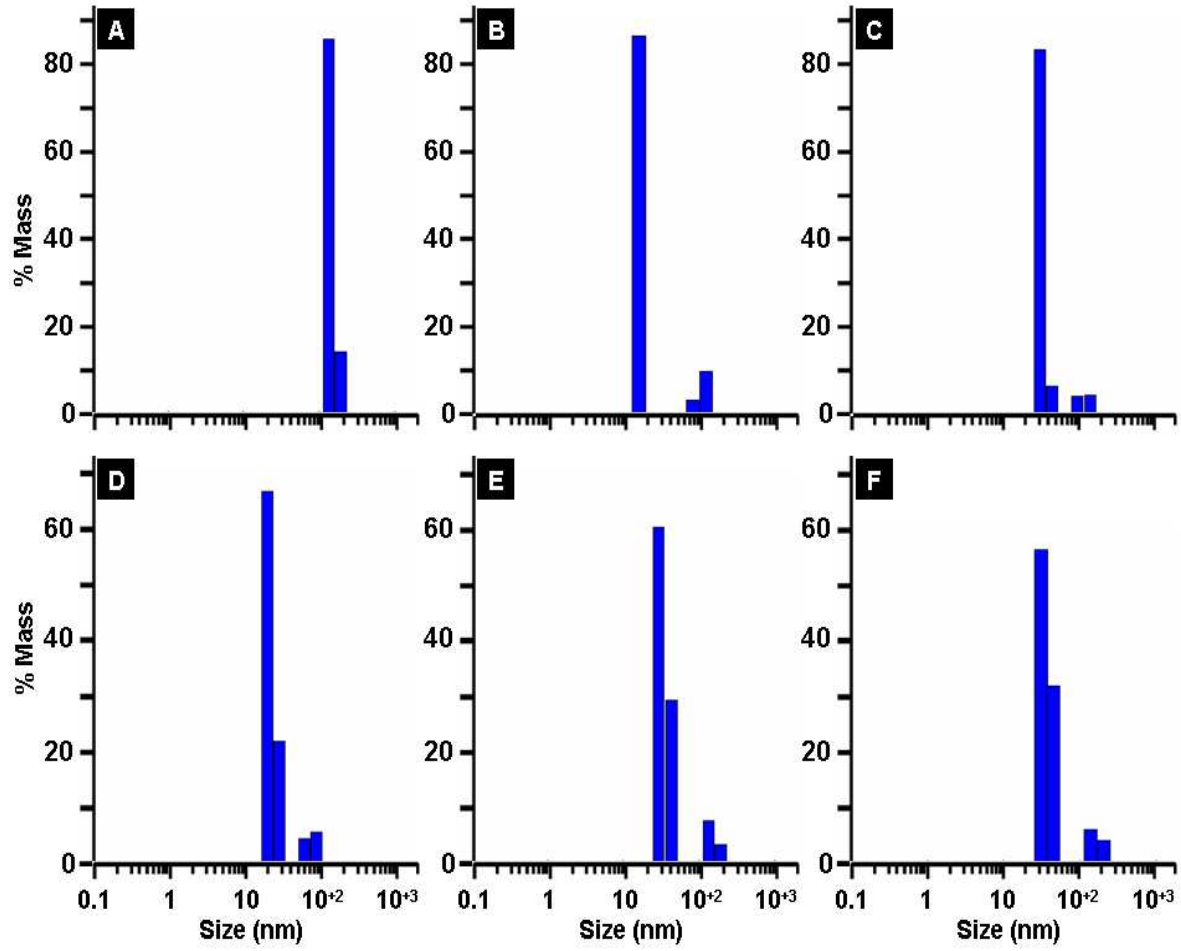

Figure 6.

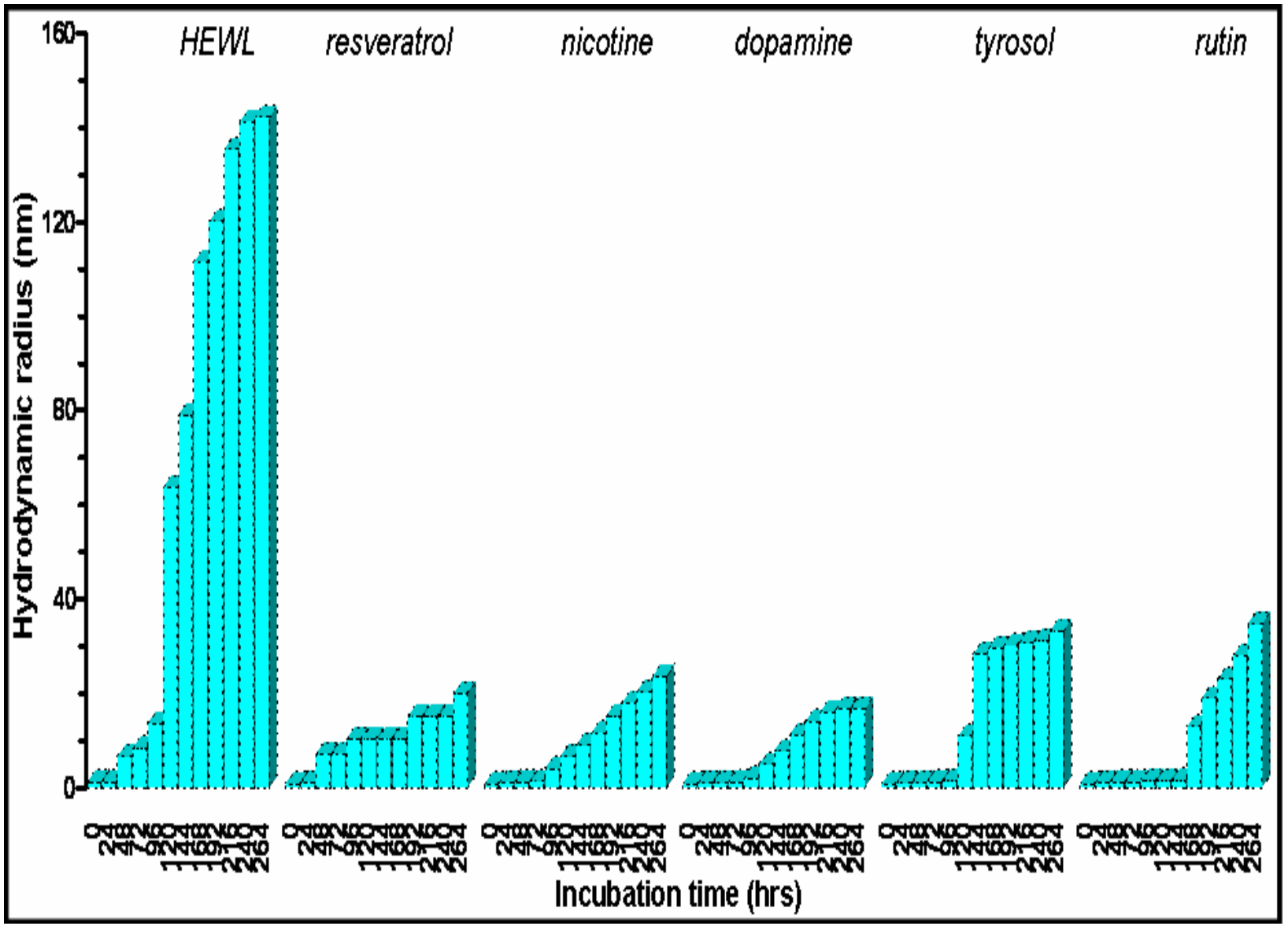
HEWL
resveratrol
nicotine
dopamine
tyrosol
rutin
Hydrodynamic radius (nm)
160
120
80
40
0
Incubation time (hrs)

Figure 7.

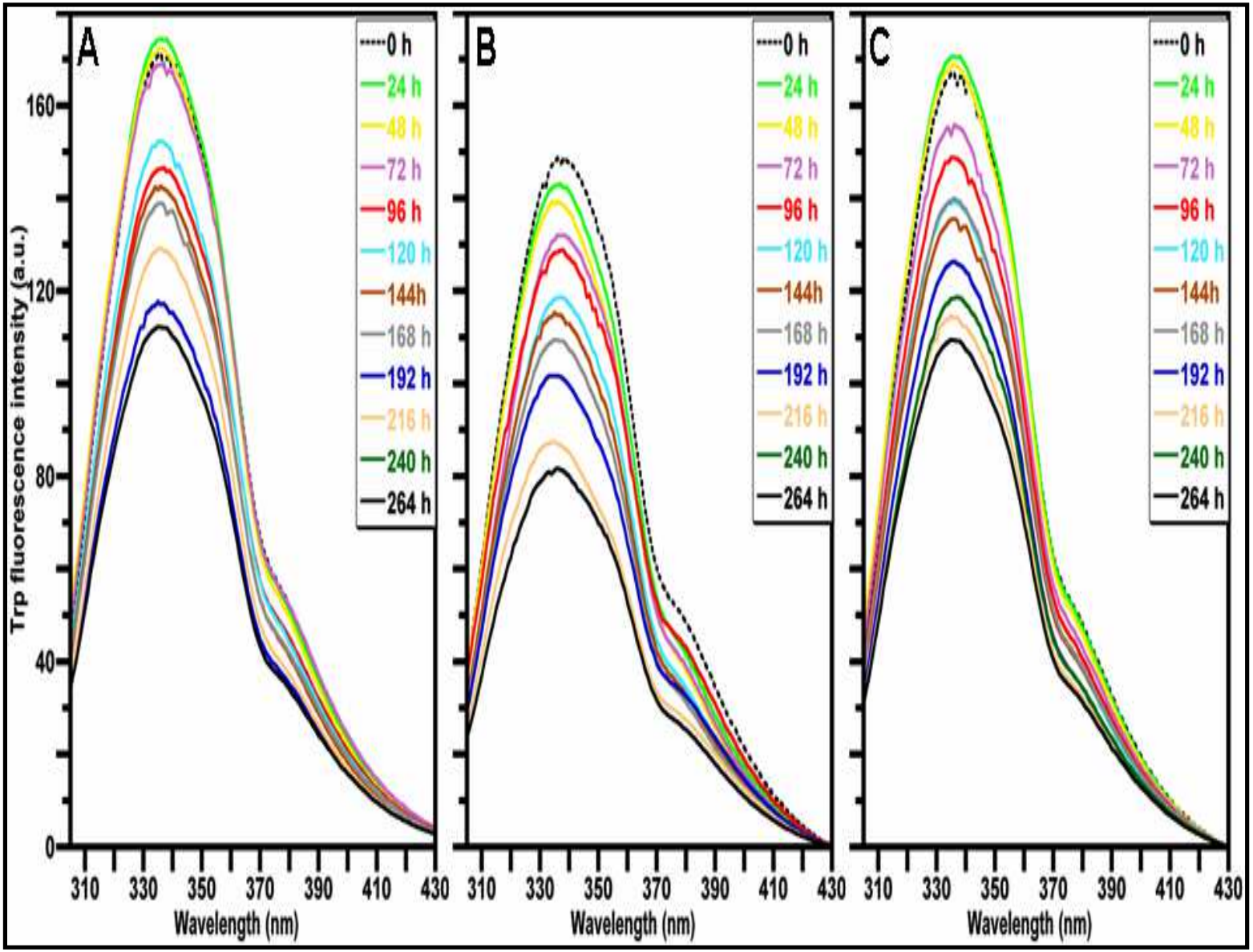
A
B
C
0 h
24 h
48 h
72 h
96 h
120 h
144h
168 h
192 h
216 h
240 h
264 h
Trp fluorescence intensity (a.u.)
0
40
80
120
160
310
330
350
370
390
410
430
Wavelength (nm)

Figure 8.

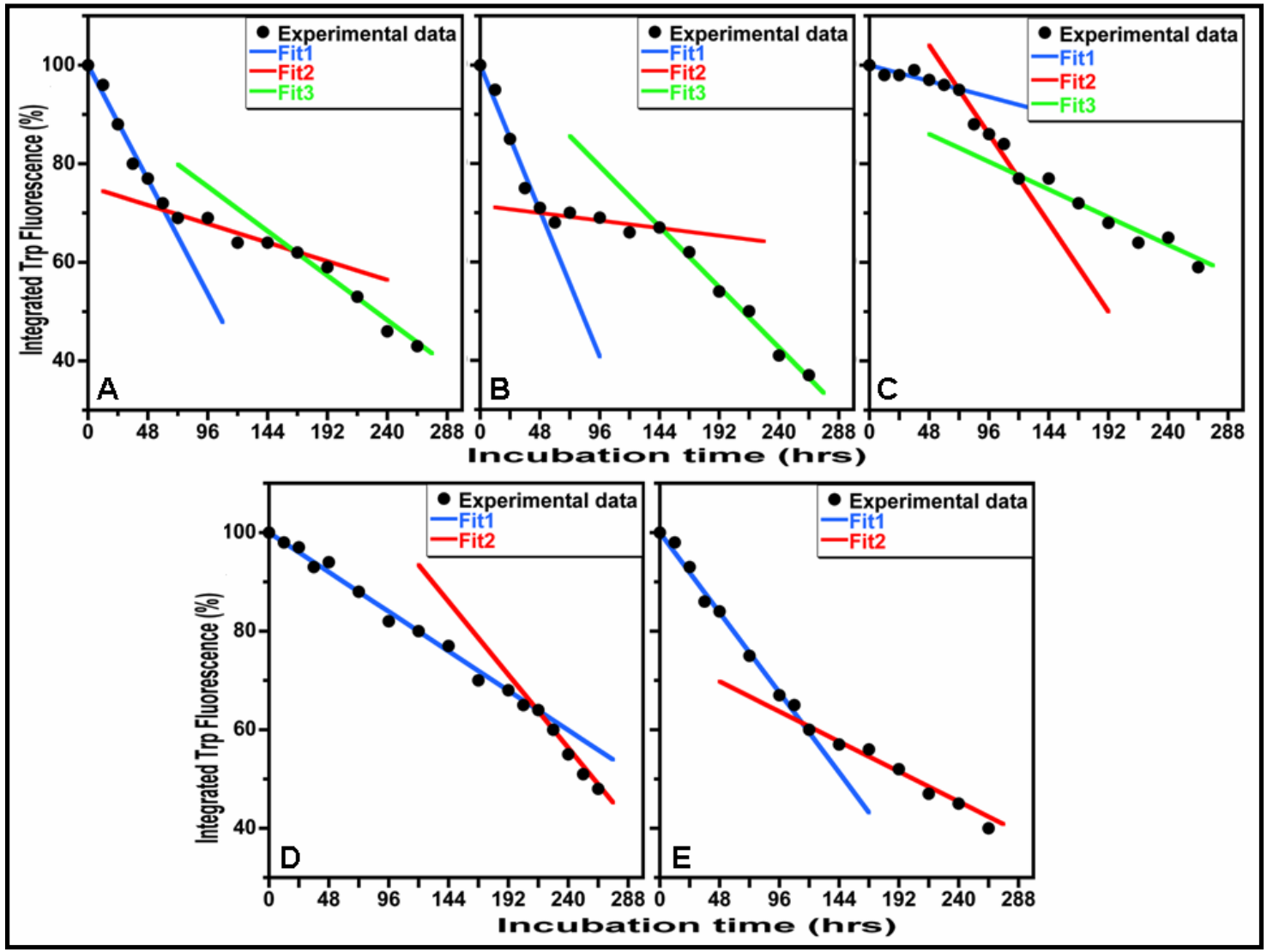
Experimental data
Fit1
Fit2
Fit3
Integrated Trp Fluorescence (%)
100
80
60
40
A
B
C
0
48
96
144
192
240
288
Incubation time (hrs)
Experimental data
Fit1
Fit2
Integrated Trp Fluorescence (%)
D
E
Incubation time (hrs)

Figure 9A

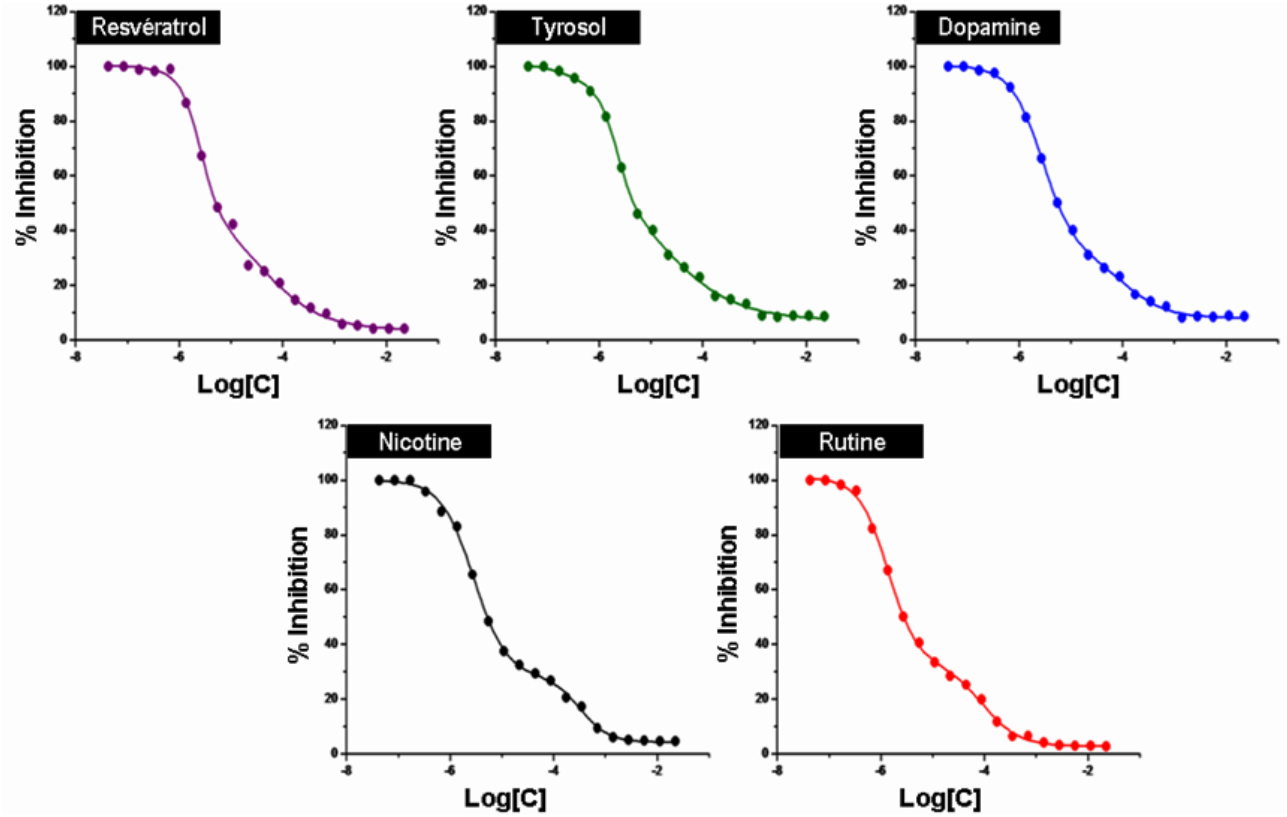
Resvératrol
Tyrosol
Dopamine
Nicotine
Rutine
% Inhibition
Log[C]

Figure 9B

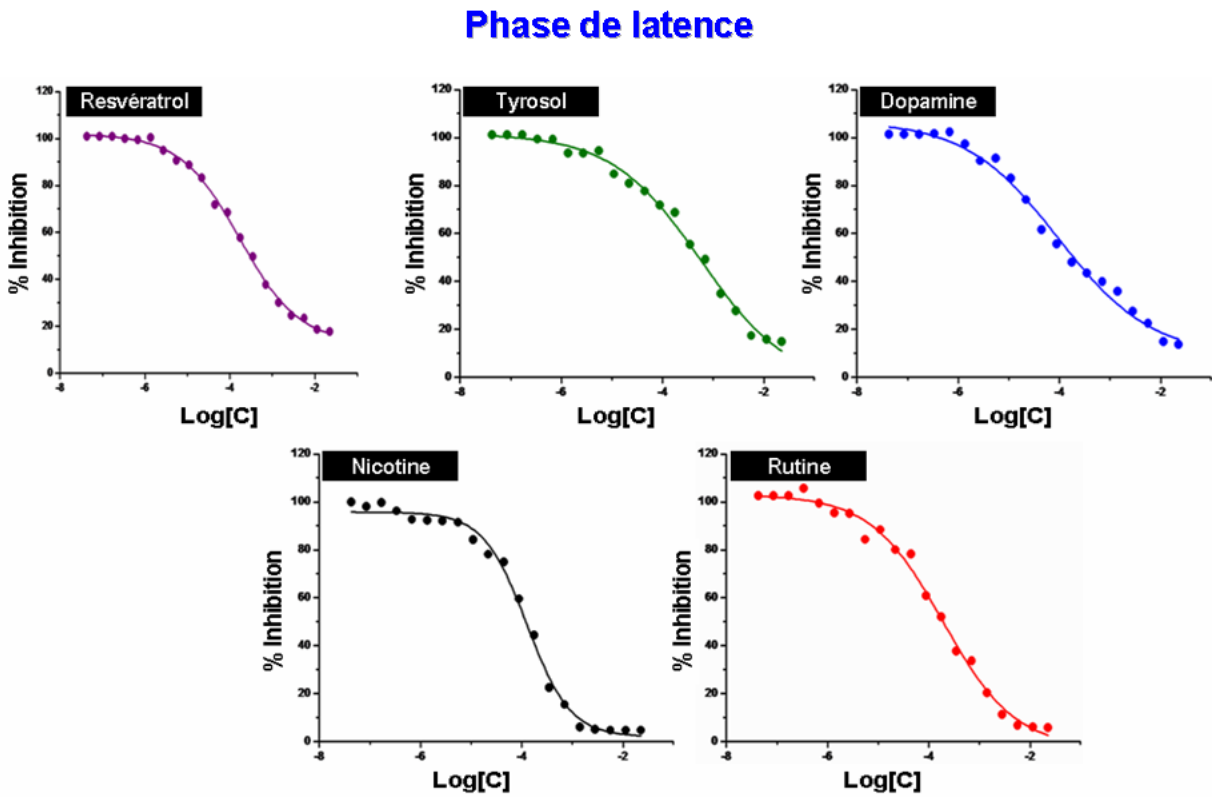
Phase de latence
Resvératrol
Tyrosol
Dopamine
Nicotine
Rutine
% Inhibition
Log[C]